

Numerical Simulation of Aerosol Concentration Effects on Cloud Spectral Evolutions of Warm Stratiform Clouds in Jiangxi, China

Yi Li^{1,2}, Xiaoli Liu^{1,2*}, Hengjia Cai^{1,2}

¹ China Meteorological Administration Aerosol-Cloud and Precipitation Key Laboratory, Nanjing University of Information Science and Technology, Nanjing 210044, China.

² College of Atmospheric Physics, Nanjing University of Information Science and Technology, Nanjing 210044, China.

Correspondence to: Xiaoli Liu (liuxiaoli2004y@nuist.edu.cn)

Abstract.

Aerosols, as cloud condensation nuclei (CCN), may impact cloud droplet spectrum relative dispersion (ϵ), affecting precipitation and climate change. However, the influence of various aerosol modes on cloud microphysics remains controversial, and this effect varies with area and cloud type. This study uses a bin microphysics scheme (WRF-SBM) to simulate a warm stratiform cloud process in Jiangxi, China, from 18:00 on December 24, 2014, to 06:00 (UTC) on December 25, 2014. Satellite observation and aircraft observation data of the same period were used to validate the simulation results, and it is shown that the numerical simulation predicted the macro and microstructure of the cloud process well. Further sensitivity experiments were conducted by increasing the concentrations of nucleation, accumulation, and coarse-mode aerosols, as well as the total aerosol concentration, to five times those of the control experiment. Additionally, an experiment was conducted by reducing the total aerosol concentration to one-fifth of the control experiment. The sensitivity experiments indicate that increased aerosol concentration promotes cloud formation and broadens the cloud droplet spectrum. In contrast, a decrease in aerosol concentration suppresses cloud formation and development. Different aerosol modes have varying effects on the cloud droplet spectrum. What's more, higher accumulation mode aerosol concentration increases small droplet concentration, while increased nucleation and coarse mode aerosol concentration favors larger droplet formation. It is also

found that the correlation between ε and volume-weighted particle size (R_v) changes from positive to negative as R_v increases. The transition in correlation is influenced by the relative strengths of cloud droplet collision-coalescence, condensation, and activation processes. The increase in accumulation mode aerosol concentration strengthens the positive correlation between ε and R_v in the R_v range of 4.5-8 μm , while the decrease in aerosol concentration strengthens the negative correlation in the same R_v range. Regardless of different coalescence intensity, ε converges with the increase in number concentration of cloud droplet (N_c). Changes in number concentration for different aerosol modes do not alter the convergence trend of ε - N_c but only affect the dispersion state of ε at low N_c levels.

1 Introduction

According to Lau and Wu (2003), warm clouds account for 32% of total precipitation in tropical regions and cover 72% of the total precipitation area. Warm clouds play a critical role in evaluating cloud-precipitation-climate feedback, making the understanding of their formation, development, and cloud microphysical processes a crucial topic in cloud physics (Zhao and Ishizaka, 2004; Seifert and Onishi, 2010).

Grosvenor et al. (2018) identified a significant relationship between cloud droplet number concentration (N_c), cloud optical thickness, and cloud top temperature, proposing an improved remote sensing retrieval algorithm for cloud droplet effective radius to reduce the errors in satellite measurements of N_c . Zheng et al. (2021) utilized merged Cloud Sat-CALIPSO-MODIS products to compare the macro- and microphysical properties of precipitating and non-precipitating clouds during the warm season in central-eastern China, focusing on parameters such as cloud optical thickness and the effective radius of cloud droplets. Their findings indicated that the probability of precipitation increased with the increasing of cloud optical thickness, liquid water path, and ice water path, but showed a decreasing trend when the cloud droplet effective radius exceeded 22 micrometres. However, these studies have overlooked the impact of changes in particle size distribution in clouds, which may

be critical for parameterization of cloud droplet effective radius and is an essential factor that cannot be ignored during cloud-rain auto-conversion processes, affecting macroscopic and microscopic physical processes in clouds (Lu et al., 2022; Xie et al., 2015).

45 Cloud droplet spectral relative dispersion (ϵ) is an important parameter that describes the width and distribution of cloud droplet sizes. It is represented as the ratio between the standard deviation (σ) and the mean radius (R_{ave}) of the droplets (Wang and Lu, 2022). On the one hand, ϵ influences the effective radius of cloud droplets and the auto-conversion process, thereby affecting cloud precipitation processes (Liu et al., 2005, 2006; Zhu et al., 2020; Lu and Xu, 2021; Wang et al., 2022; Wang et al., 2023; Yang et al., 2023). On the other hand, ϵ affects cloud-aerosol interactions, impacting climate (Xie et al., 2017).

50 Many researchers have conducted causal analyses on the uncertainty of the effect of cloud microphysical properties on ϵ . The results indicate that the variability of ϵ is influenced by various factors, such as atmospheric temperature, humidity, and entrainment (Lu et al., 2013). Zhu et al. (2020) analysed data from a flight observation conducted in Monterey, California, in July 2008 as part of the US POST (Physics of Stratocumulus Top) project, found that in adiabatic clouds, vertical velocity plays a dominant role, and an increase in vertical velocity promotes the activation of cloud condensation nuclei (CCN), leading
55 to an increase in N_c and facilitating droplet coalescence and growth. On the other hand, Kumar et al. (2017) conducted idealized simulation experiments using direct numerical simulation (DNS) to study the mixing dynamics at cloud edges and their impact on the droplet size distribution (DSD). They showed that ϵ is also related to turbulent mixing and variations in vertical velocity within the cloud.

However, as Lu et al. (2020) pointed out, existing studies on ϵ primarily rely on empirical data from observations, leading
60 to significant uncertainty in characterizing the ϵ within clouds. In addition, the relationship between the ϵ and the volume-mean radius (R_v) has shown varied conclusions in different studies: some indicate a negative correlation (Liu et al., 2008; Pandithurai et al., 2012), while others suggest a positive correlation (Tas et al., 2012). It is also found that as R_v increases, the

ε exhibits a converging trend (Chen et al., 2016). Meanwhile, the correlation between the ε and N_c also shows uncertainty. Jin et al. (2021) conducted aircraft observational studies on stratiform warm clouds in Jiangxi, China, indicating that ε in both precipitating and non-precipitating warm clouds is negatively correlated with N_c . But, some studies report a positive correlation (Pandithurai et al., 2012; Chen et al., 2016), while others indicate a negative correlation (Cecchini et al., 2017; Wang et al., 2011). Some studies even suggest that no significant correlation is observed between ε and N_c (Tas et al., 2015). Meanwhile, the correlation between ε and N_c also shows uncertainty. Jin et al. (2021) conducted aircraft observational studies on stratiform warm clouds in Jiangxi, China, indicate that ε in both precipitating and non-precipitating warm clouds is negatively correlated with N_c . Similarly, Cecchini et al. (2017) and Wang et al. (2011) reported negative correlations between ε and N_c . However, some studies report a positive correlation (Pandithurai et al., 2012; Chen et al., 2016). While some studies even suggest that no significant correlation is observed between ε and N_c (Tas et al., 2015).

Studies by Ma et al. (2010) and Wang et al. (2011, 2019) have shown that changes in ε are highly sensitive to aerosol concentration and its activation process. Additionally, alterations in aerosol concentration or size distribution significantly impact the cloud-rain auto-conversion process through ε changes. Consequently, ε becomes a critical link connecting the aerosol-cloud interaction effects (Liu and Daum, 2002).

Liu et al. (2003) compared aircraft observations and satellite retrievals for warm clouds in both the northern and southern hemispheres and found that an increase in aerosol concentration leads to a decrease in cloud droplet effective radius and narrowing of the droplet spectrum, thus suppressing warm precipitation processes. Fan et al. (2012) conducted a numerical simulation on variations of aerosol concentration in Eastern China, demonstrating that an increase in CCN leads to an increase in N_c and cloud droplet mass concentration, reduces the number concentration of raindrops, and delays the onset of precipitation. Yang et al. (2017) analysed aerosol concentration and cloud droplet spectrum distribution in the high-altitude region of eastern China during summer, and the results showed that increased aerosol concentration inhibits the cloud-rain

auto-conversion process, resulting in more cloud water remaining in the atmosphere and reducing warm precipitation. By
85 analysing the aerosol observations in India from 2000 to 2017, Kant et al. (2019) found that strong updrafts with abundant
mineral dust aerosols can activate more cloud droplets, leading to competition for water vapor and narrowing the droplet
spectrum, limiting the growth of high-level liquid droplets. It is suggesting that an increase in aerosol concentration leads to a
reduction in ϵ , thereby inhibiting the cloud-rain auto-conversion process (Chandrakar et al., 2016, 2018; Desai et al., 2019).

However, there are also studies indicating that an increase in aerosol concentration results in an increase in ϵ and enhances
90 droplet collision-coalescence processes (Rotstayn and Liu, 2003; Yum and Hudson, 2005; Rotstayn and Liu, 2009; Prabha et
al., 2012; Liu et al., 2020). For instance, Liu et al. (2020) found that increasing aerosol concentration in clean tropical or marine
regions can prolong cloud lifetimes and enhance precipitation by modifying the cloud droplet spectrum distribution. Moreover,
it is found that the influence of aerosol concentrations on cloud droplet size distribution exhibits strong regional dependence,
varies according to cloud types and geographical regions (Chandraka et al., 2016; 2018).

95 In addition, the impact of aerosol concentrations on cloud droplet spectrum varies for different size ranges of aerosols.
Liu et al. (2022), using satellite data to investigate the influence of aerosols on warm cloud processes, found that fine particles
with diameters ranging from 0.1 to 2.5 micrometres, acting as cloud condensation nuclei, can suppress precipitation and
prolong the lifetime of maritime warm clouds, like the conclusions of Kovačević (2018) and Lerach and Cotton (2018). On
the other hand, an increase in coarse-mode marine condensation nuclei with larger particle sizes leads to a noticeable increase
100 in cloud droplet effective radius and warm rain intensity. It is found that large particles with diameters exceeding 2 micrometres,
acting as giant cloud condensation nuclei, can increase ϵ and facilitate cloud droplet growth during the collision-coalescence
process (Yin et al., 2000; Jensen and Nugent, 2017). However, Wehbe et al. (2020) analysed aircraft observations over the
United Arab Emirates in 2019, and found that although giant cloud condensation nuclei were present, no significant collision-
coalescence process was observed in warm clouds.

105 Furthermore, Rosenfeld et al. (2001) attributed the reduction in cloud droplet effective radius over the Sahara Desert to numerous submicron-sized cloud condensation nuclei (CCN), which decreased ε exacerbated the decrease in precipitation over the Sahara region. Numerical experiments by Flossmann and Wobrock (2010) yielded similar conclusions.

 In summary, under the context of climate change, changes in the physicochemical properties of aerosols significantly affect the microphysical characteristics of warm clouds. Existing studies often rely on exploring the relationships between
110 aerosol concentration and microphysical cloud quantities such as N_c and R_v , and further research on ε , a key factor affecting the cloud-aerosol effect, is still needed. However, the response of warm clouds to aerosol physicochemical properties depends on the region and cloud type, and due to limitations in observational methods, the response of ε to changes in aerosol concentration varies significantly across studies, making this issue a crucial and controversial scientific question in climate prediction.

115 This study utilizes the SBM-FAST bin microphysics scheme within the Weather Research and Forecasting (WRF) model to simulate a stratiform warm cloud event in Jiangxi, China. The numerical experiments aim to explore the impacts of changes in nucleation, accumulation, coarse, and total mode aerosol concentrations on the macroscopic and microscopic characteristics of warm clouds in this region. The paper is organized as follows: Section 2 outlines the numerical simulation setup, aircraft, and satellite observations to validate simulation results, and the computational formulas used in the analysis, the third section
120 3 conducts validations of the control experiment's simulation results through comparisons with concurrent aircraft and satellite cloud top temperature observations, uncovering the effects of different aerosol modes on the macroscopic and microscopic physical properties of clouds, with a particular focus on the correlation between ε and cloud microphysical properties. The last two section include the discussion and conclusions.

2 Model Introduction and Experiment Design

125 2.1 Simulation Setup and Weather Conditions

This paper selects a warm cloud process that occurred in the Jiangxi, China on December 25, 2014, and conducts simulations using the WRF (Weather Research and Forecasting) 4.2 version. The experiment comprises one control and five aerosol spectrum modification experiments. Except for aerosol concentrations, all groups keep the initial field data and simulation settings consistent. The simulations use the fifth generation of ECMWF atmospheric reanalyses of the global climate (ERA5) hourly data on pressure levels as the initial field, with a resolution of $0.25^{\circ} \times 0.25^{\circ}$.

The simulations employ a two-layer nesting approach with 3 km and 1 km grid resolutions. The model is divided vertically into 57 layers, reaching a top pressure level of 50 hPa, and the innermost layer grid measure contains 376×376 grid points. The microphysics scheme used is the new version of SBM-fast bin scheme (FSBM-2) under the WRF 4.2 version. The boundary layer scheme selected is the Mellor-Yamada-Janjic (Eta) Turbulence Kinetic Energy (TKE) scheme, and the near-
135 surface layer scheme uses the Monin-Obukhov (Janjic Eta) scheme. The land surface process adopts the unified Noah land-surface model. The (old) Goddard shortwave radiation scheme is used, and the Rapid Radiative Transfer Model (RRTM) scheme is chosen for longwave radiation.

The simulation region is illustrated in Figure 1, and the simulation duration is from 18:00 on December 24, 2014, to 06:00 on December 25, 2014 (UTC), with no precipitation was observed at the ground during the simulation period. The simulated
140 area, Ganzhou City, is in the southern part of eastern China's Jiangxi province. It is located upstream of the Gan River and in the transitional zone between the southeastern coastal and central inland regions. The city is surrounded by mountains, with faulted basins traversed. The predominant topographical features are mountains, hills, and basins. The area is located at the southern edge of the subtropical zone and falls under the subtropical monsoon climate region.

As shown in Figure 2, at 00:00 on the 25th, a high-altitude trough shifted eastward, with the mid-level located in the southwest jet stream, which was relatively weak. At the 850hPa level, the Jiangxi region near the flight area displays a convergent wind field, indicating the presence of ascending air currents. The wind speeds are relatively low, and the upward motion is gentle.

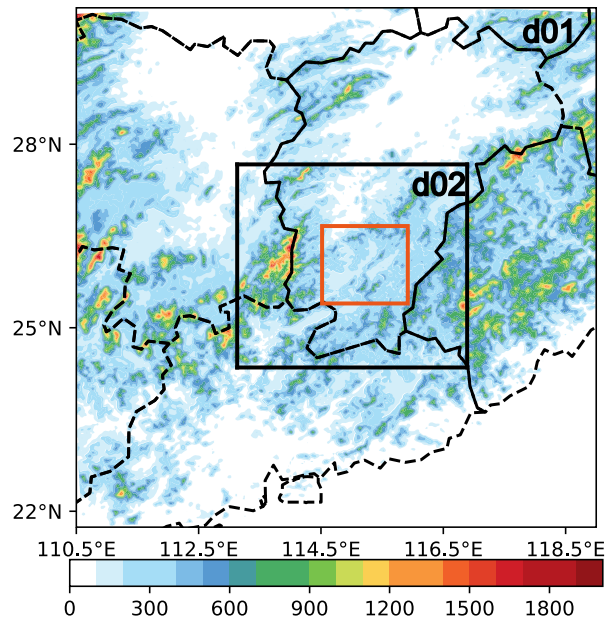


Figure 1: Simulated Region and Nesting Configuration. The shading represents the elevation (m) of the terrain, and the area within the red box is the analysis range.

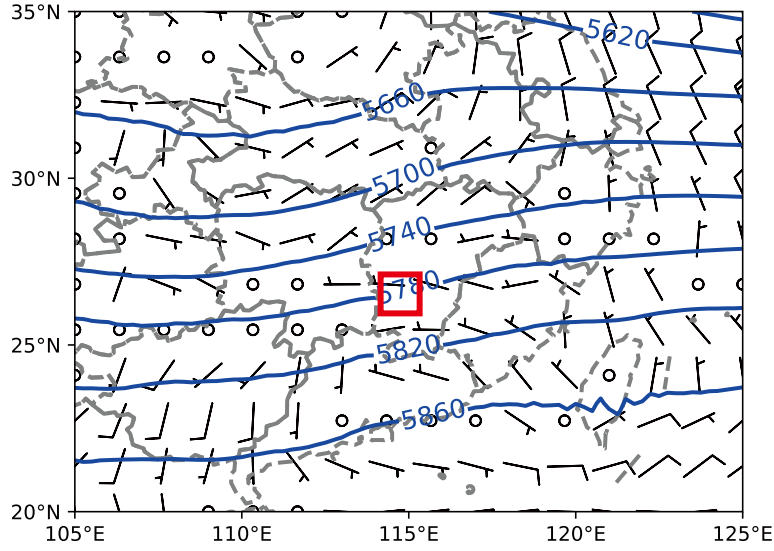


Figure 2: The 500 hPa geopotential height field (blue contour lines, unit: dagpm) and the 700 hPa wind field (wind barbs) at 00:00 (UTC) on December 25, 2014. The area within the red box indicates the starting point of the flight.

2.2 Introduction to Microphysics Scheme

155 The SBM-fast scheme was initially developed by Khain and Lynn (2009) as a simplified version of the SBM-full bin scheme based on the original microphysics scheme included in the Hebrew University Cloud Model (HUCM) (FSBM-1) (Khain and Sednev, 1996; Khain et al., 2000). The FSBM-2 used in this study is an improvement over FSBM-1 by Shpund et al. (2019) and has been verified to exhibit better simulation performance (Han et al., 2019).

In FSBM-2, cloud and rain droplets are described using a unified liquid droplet bin scheme, which is divided into 33 bins.

160 The aerosol scheme is divided into marine and continental components, and the aerosol spectrum distribution is described using 43 or 33 mass bins. Regardless of whether 33 or 43 aerosol bins are used, the maximum dry aerosol radius is set to $2\mu\text{m}$. The scheme activates aerosols into liquid droplets under supersaturation conditions (cloud nucleation: Pinsky and Khain, 2018). In the model, the minimum CCN size is assumed to be $0.003\mu\text{m}$, and the initial aerosol distribution is represented by the sum of three lognormal distributions, corresponding to the nucleation mode (centered at $0.008\mu\text{m}$), accumulation mode (centered at $0.034\mu\text{m}$), and coarse mode (centered at $0.46\mu\text{m}$). The calculation of cloud droplet nucleation considers the effect of

165

supersaturation, and the algorithm's accuracy is verified through comparison with large-eddy simulation results (Ilotoviz et al., 2015).

2.3 Sensitivity Experiment Configuration

This paper includes five aerosol concentration modification experiments and one control experiment (ORG). The initial aerosol concentrations set in the control experiment, are shown in Table 1. The initial aerosol concentrations are modified for the other five experiment, as shown in Table 2. According to the aircraft observational study on the impact of aerosol concentration changes on precipitation in Eastern China (Qian et al., 2009) and the numerical simulation study on the effect of aerosol concentration changes on clouds and precipitation in Eastern China (Fan et al., 2012), increasing the initial aerosol concentration to five times realistically reflects the background concentration of continental aerosols under polluted conditions in Eastern China. This adjustment is beneficial for demonstrating the realistic impacts of aerosol concentration changes on warm clouds in eastern China. Experiments 1, 2, and 3, modify the aerosol concentrations of the nucleation mode (NM), accumulation mode (AM), and coarse mode (CM) to five times their original values, respectively. Experiment 4 (ITM) simultaneously modifies the aerosol concentrations of the nucleation, accumulation, and coarse modes to five times their original values, and experiment 5 (DTM) reduces the aerosol concentrations by five times compared to the original group. The initial background aerosol spectrums in the simulations are shown in Figure 3.

Table 1: Initial Aerosol Concentration in the Control Experiment.

Aerosol Types	Number Concentration (cm ⁻³)	Mean Particle Size (μm)
Nucleation Mode	1000	0.008
Accumulation Mode	800	0.034
Coarse Mode	0.720	0.460

Table 2: Initial Aerosol Concentration Settings in Sensitivity Experiments.

	Nucleation Mode (cm ⁻³)	Accumulation Mode (cm ⁻³)	Coarse Mode (cm ⁻³)
Experiment 1 (NM)	5000	800	0.720
Experiment 2 (AM)	1000	4000	0.720
Experiment 3 (CM)	1000	800	3.600
Experiment 4 (ITM)	5000	4000	3.600
Experiment5 (DTM)	200	160	0.144

185

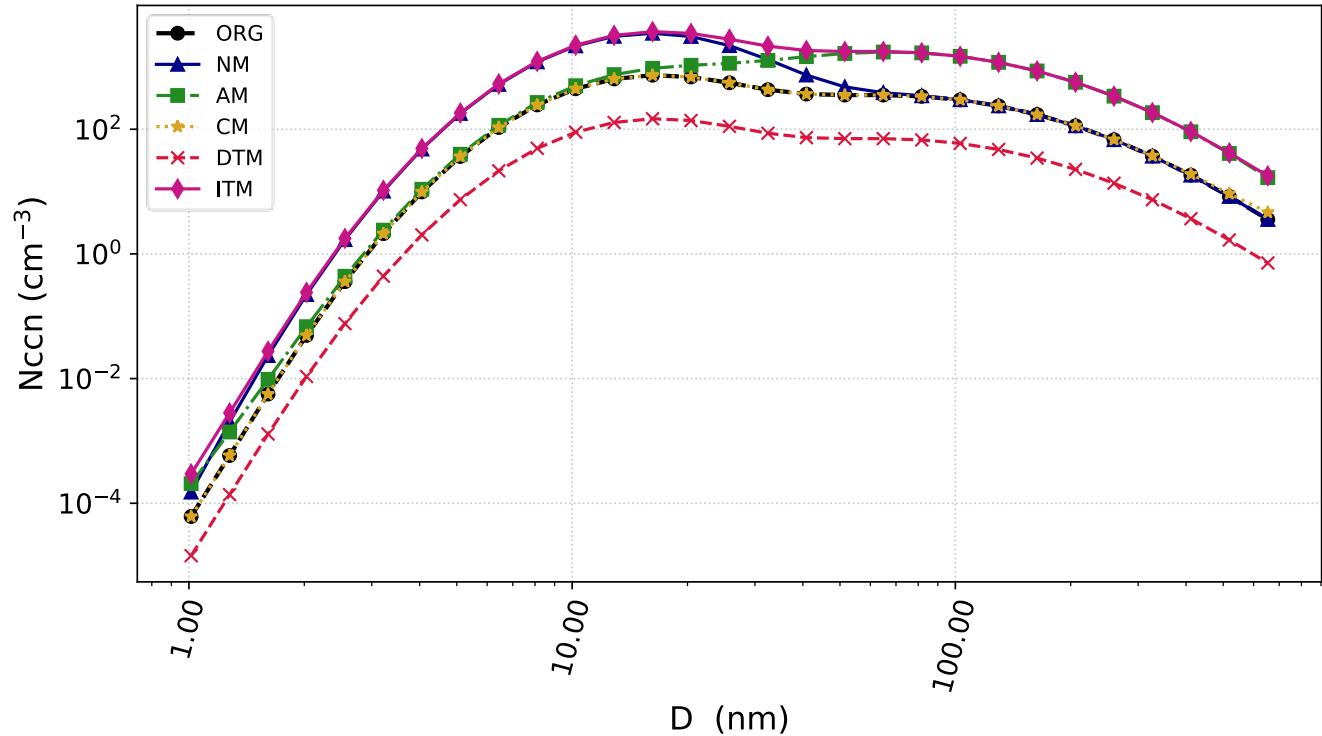


Figure 3: Initial aerosol number concentration (unit: cm⁻³) as a function of particle diameters (unit: nm).

2.4 Calculation of Cloud Droplet Spectrum Parameters

In this study, the changes in cloud droplet spectrum and cloud droplet spectral parameters were analysed. The mean cloud
190 droplet Radius (Rm), Rv, cloud-rain auto-conversion threshold (T), ε, and cloud droplet activation intensity (Fbs) were
calculated as shown in Supplement.

2.5 Introduction of Data

2.5.1 Introduction of Aircraft Observation Data

The aircraft observation data used in this study were sourced from a flight observation mission conducted in Jiangxi, China on December 25, 2014. Observations were carried out using the Yun-12 aircraft equipped with a comprehensive set of aerosol-cloud-precipitation detectors. The cloud microphysical data were obtained from the Cloud-Aerosol Spectrometer (CAS), while flight altitude and path information were obtained from the Aircraft Integrated Meteorological Measurement System (AIMMS-20). To ensure the accuracy and reliability of the observation data, all probes and the observation platform were precisely calibrated prior to the observations, and outliers were removed from the post-observation data.

The observation flight area was located above Ganzhou City in Jiangxi Province, spanning coordinates from 114.0°E to 117.0°E and from 25°N to 27°N. The flight trajectory, shown in Figure 4, details the specific path of the observation. The aircraft took off from Ganzhou Airport and followed a flight pattern that included ascending, cruising, and spiralling down. The flight lasted from 01:29 to 04:45 (UTC), reaching a maximum altitude of 4126 meters. To exclude data from non-cloud areas during the observation period, a cloud region criterion of cloud liquid water content (Clw) $> 0.001 \text{ g/m}^3$ and number concentration of cloud droplets (Nc) $> 10 \text{ particles cm}^{-3}$ was applied (Jin et al. 2021).

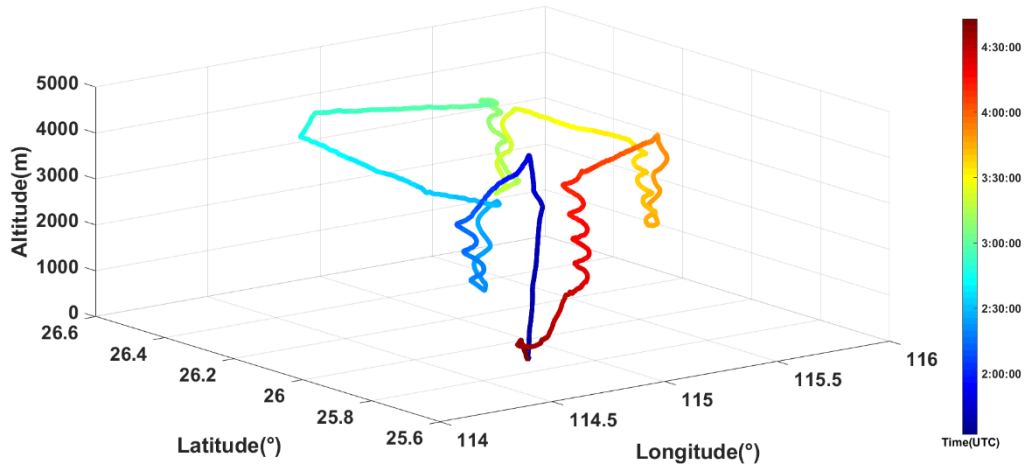


Figure 4: The flight track of the observing aircraft on December 25, 2014, with colors of the line representing the flight time.

2.5.2 Introduction to Satellite-Observed Cloud Top Temperature Data

This work utilizes the standard format cloud top temperature full-disk scan data provided by the FY-2F meteorological satellite of the National Satellite Meteorological Center, covering November to December 2014. The FY-2F satellite's scanning radiometer includes five channels. The cloud top temperature data used in this study come from the VISSR-II channel, which has a spatial resolution of 5 km, a temporal resolution of 1 hour, and a valid data range from 0 to 400 K.

3 Results and analysis

3.1 Simulation Results Validation

To verify the simulation performance of the control experiment, we compared the simulated results with cloud-top temperature observations from the FY-2F satellite and aircraft observations on December 25, 2014.

Figure 5 shows that the control experiment and satellite data both show band-like warm cloud regions with cloud-top temperatures ranging from 5 to 10°C in the central and northern parts of Jiangxi. It is shown that the distribution of observed and simulated cloud-top temperatures is quite similar.

220 Aircraft observation data on December 25, 2014, in Jiangxi region was chosen to further validate the simulated vertical distribution of cloud microphysical characteristics. The data was obtained from the CAS probe onboard the aircraft, which measures aerosols and cloud particles with diameters ranging from 0.51 to 50 μm , covering 30 bins with varying size bins. The observation period was from 01:35 to 04:45 (UTC) on December 25, 2014. During the observation period, the warm cloud within the flight area had a maximum horizontal extent of over 50 kilometres, and it was characterized as a stratiform warm
225 cloud process. For the control experiment, the cloud water content, cloud droplet number concentration, and average cloud droplet diameter were compared in the same observation duration and flight regions.

Figure 6 shows the flight trajectory and the cloud liquid water content along the observation path. To validate the control experiment's simulation results, a comprehensive cloud penetration segment from 04:10 to 04:20 UTC was selected. During this period, the Clw, Nc, and Rm were calculated and compared with the simulation results in the same region and time frame,
230 as illustrated in Figure 7. To minimize the impact of differing vertical resolutions between aircraft observation data and model simulations, the cloud base height within the validation interval was set to 0 and the cloud top height to 1, thus achieving height normalization. Both the control experiment and the observational data exhibit an initial increase followed by a decrease in Clw and Nc with altitude. Additionally, the average particle size in both results increases with height, and their vertical distribution trends are consistent.

235 Overall, regarding the distribution of warm clouds and the vertical distribution of cloud microphysical properties, the simulation results are generally consistent with the observed data. Therefore, the simulation results are reliable.

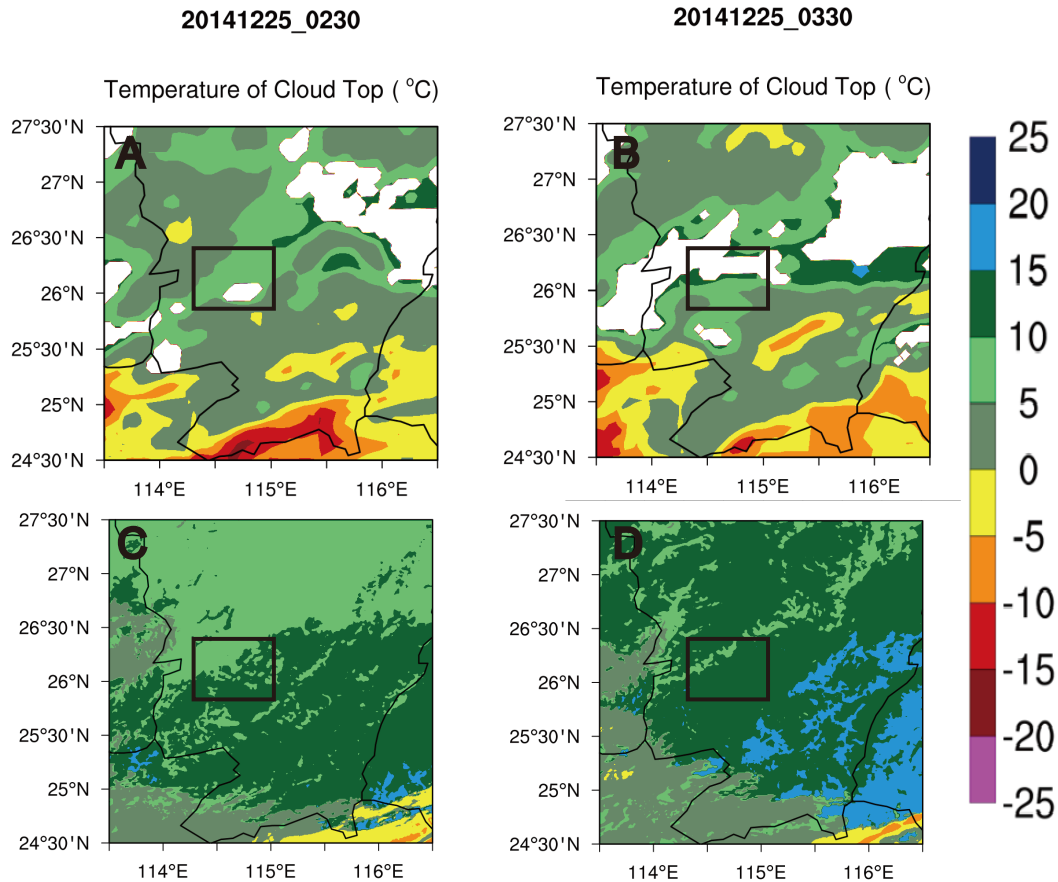


Figure 5: FY-2F satellite observed (A at 02:30, B at 03:30) and control experiment simulated (C at 02:30, D at 03:30) cloud-top temperatures on December 25, 2014 (unit: °C). The black box indicates the aircraft observation area.

240

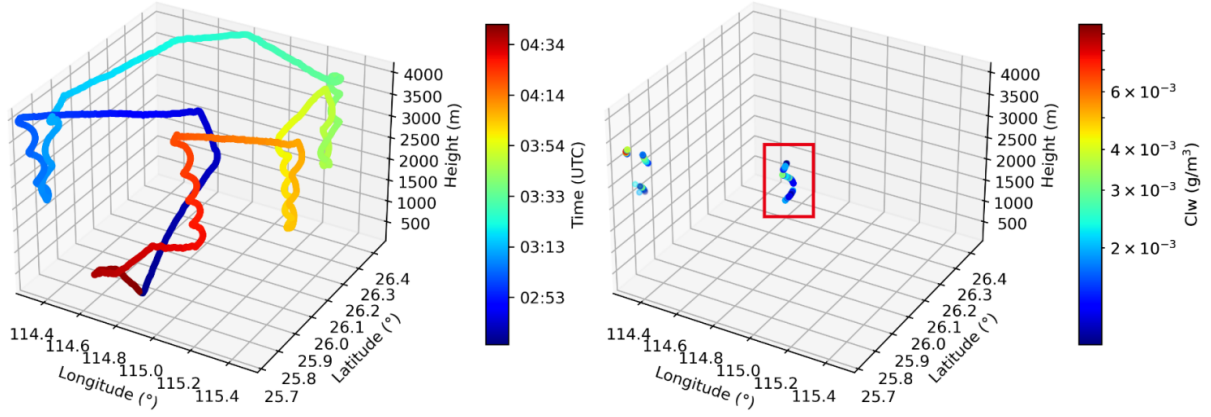


Figure 6 Aircraft flight trajectory and cloud liquid water content (Clw) within the cloud region along the observation path. The red box indicates a comprehensive cloud penetration process from 04:10 to 04:20 UTC.

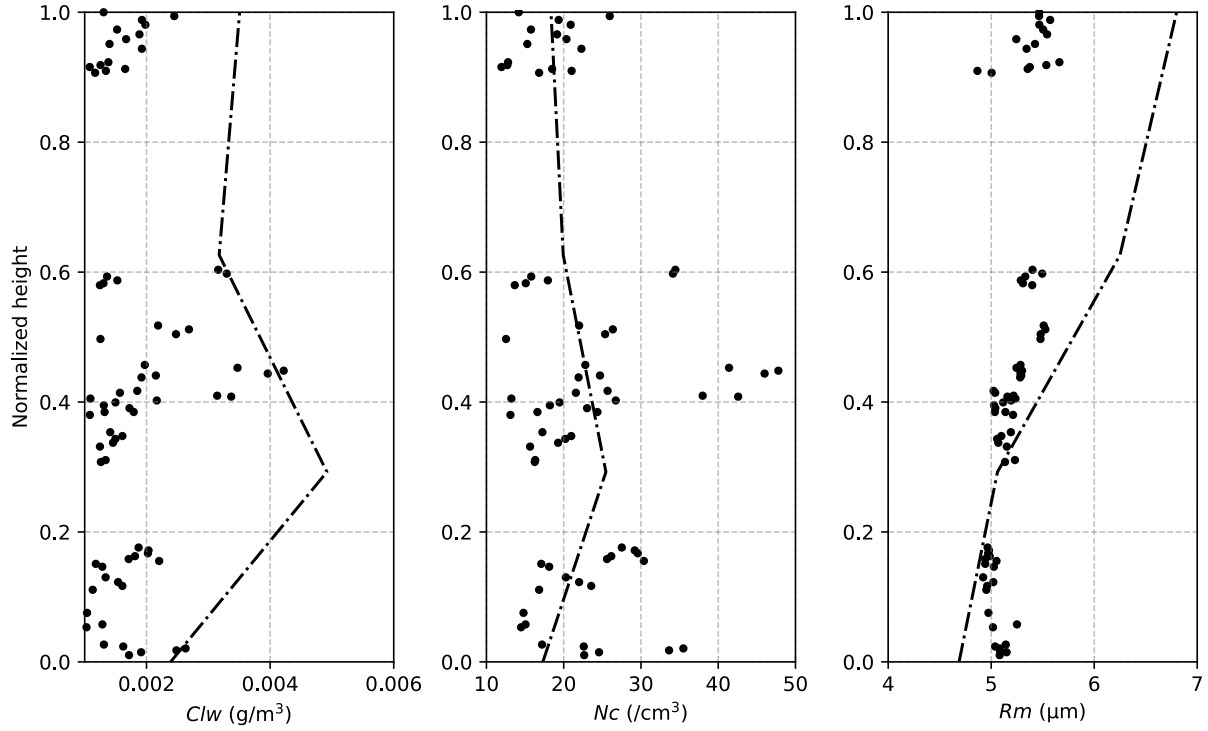


Figure 7: Aircraft observations (scatter points) of cloud liquid water content (Clw, in g/m^3), cloud droplet number concentration (Nc, in cm^{-3}), and cloud droplet mean radius (Rm, in μm) on December 25, 2014, compared with model simulations (black dashed lines) of Clw, Nc, and Rm.

245

3.2 Analysis of the Impact of Background Aerosols on Warm Cloud Properties

3.2.1 Vertical Distribution of Cloud Microphysical Properties

Figure 8-10 reflects that the cloud thickness significantly increases as the cloud system develops. Both Clw and Rm increase
250 with height, show high consistency. In contrast, Nc exhibits different trends with height at different times. From 00:00 to 02:00
UTC, when the cloud system is in initial stage of development, Nc decreases with height, and many small cloud droplets
appear at the cloud base, which is the main area for droplet activation. As the cloud system further develops, from 03:00 to
04:00 UTC, Nc shows relative uniform distribution with height. From 04:00 to 05:00 UTC, this trend changes again, with the
maximum Nc appearing at the cloud base. Large numbers of small cloud droplets present at the cloud base, the primary area
255 for droplet activation. The peak of Clw appears at higher cloud layers. In contrast, the maximum cloud droplet radius occurs
in the middle to upper cloud layers, indicating that the main region of cloud droplet size increasing is near the top and middle-
upper parts of cloud regions.

Compared to the control experiment, the increase in aerosol concentration promotes cloud development. This
phenomenon is consistent with the findings of Khain et al. (2005) and Morrison et al. (2018). When the accumulation mode
260 aerosol concentration increases, this "promoting" effect becomes most evident. On the other hand, when aerosol concentration
decreases, cloud development is suppressed, resulting in a noticeable decrease in cloud-top height.

In terms of cloud microphysical properties, with an increase in aerosol concentration, Nc noticeably increases. As a result,
more cloud droplets of small sizes compete for water vapor, reducing cloud droplet size. The maximum Nc and minimum
cloud droplet size are observed in the ITM and AM experiments. However, with aerosol concentration decreased, despite cloud
265 development being restrained, the DTM experiment exhibits the largest cloud droplet size.

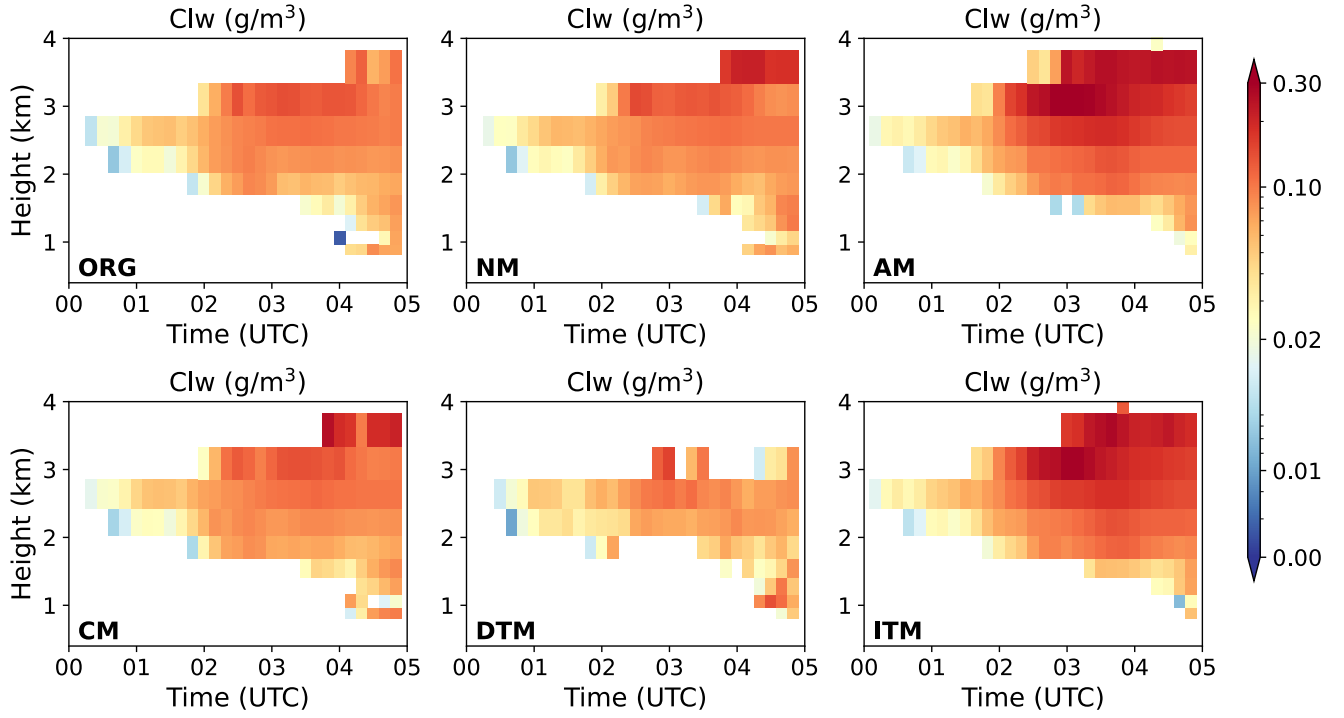
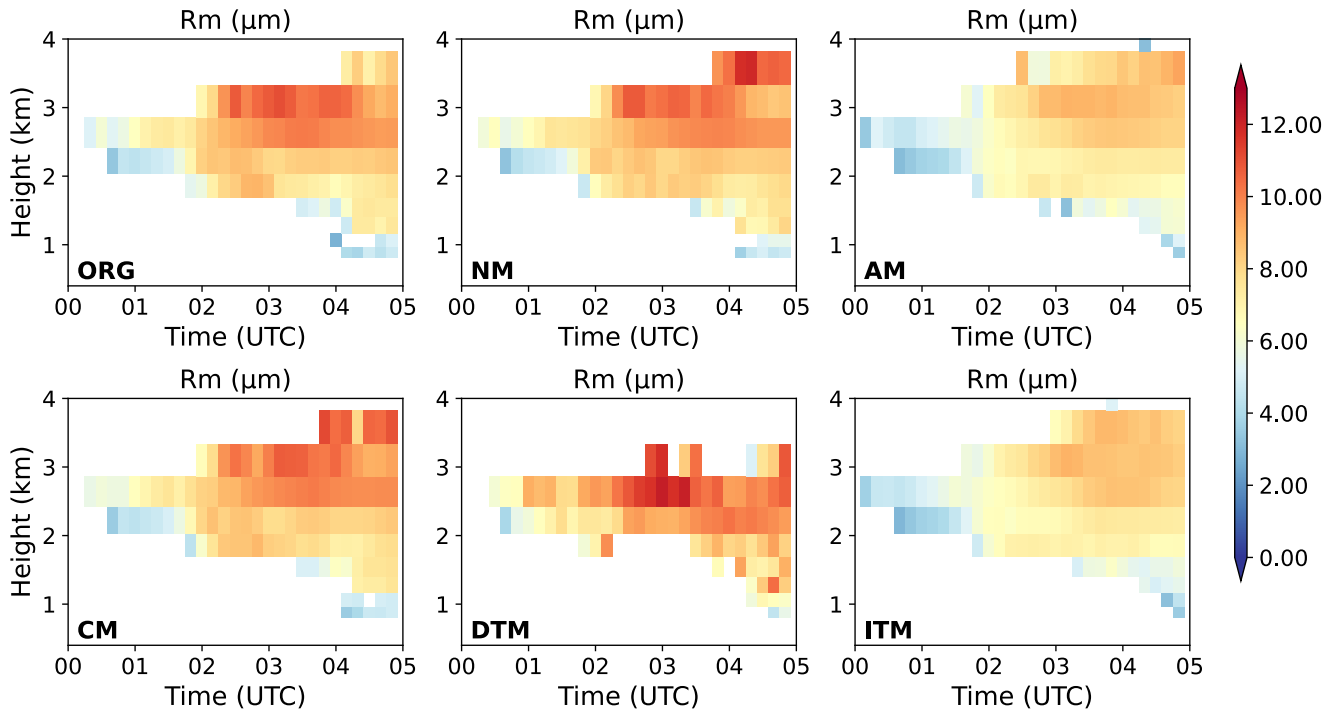


Figure 8: The variations of averaged cloud liquid water content (Clw, in g/m^3) with time (UTC) and altitude (km) within the study area of different experiments.



270 **Figure 9: The variations of averaged cloud droplet radius (R_m , in μm) with time (UTC) and altitude (km) within the study area of different experiments.**

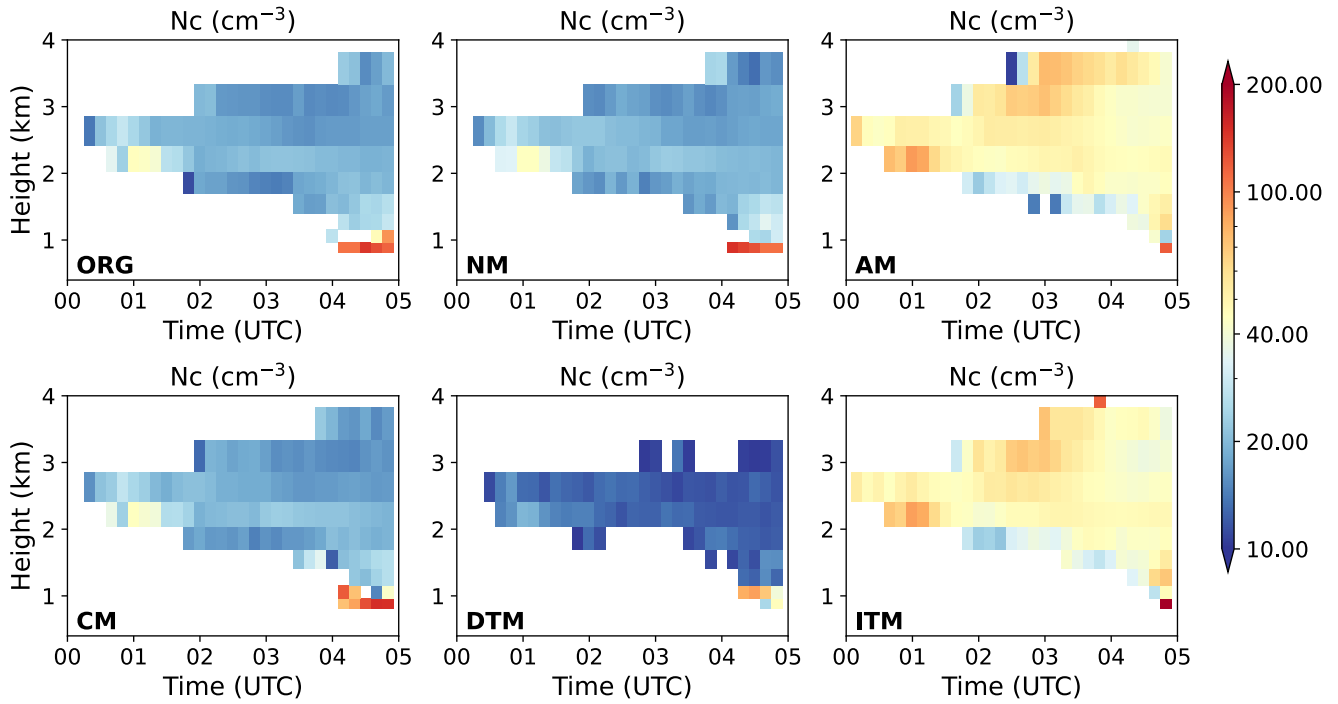


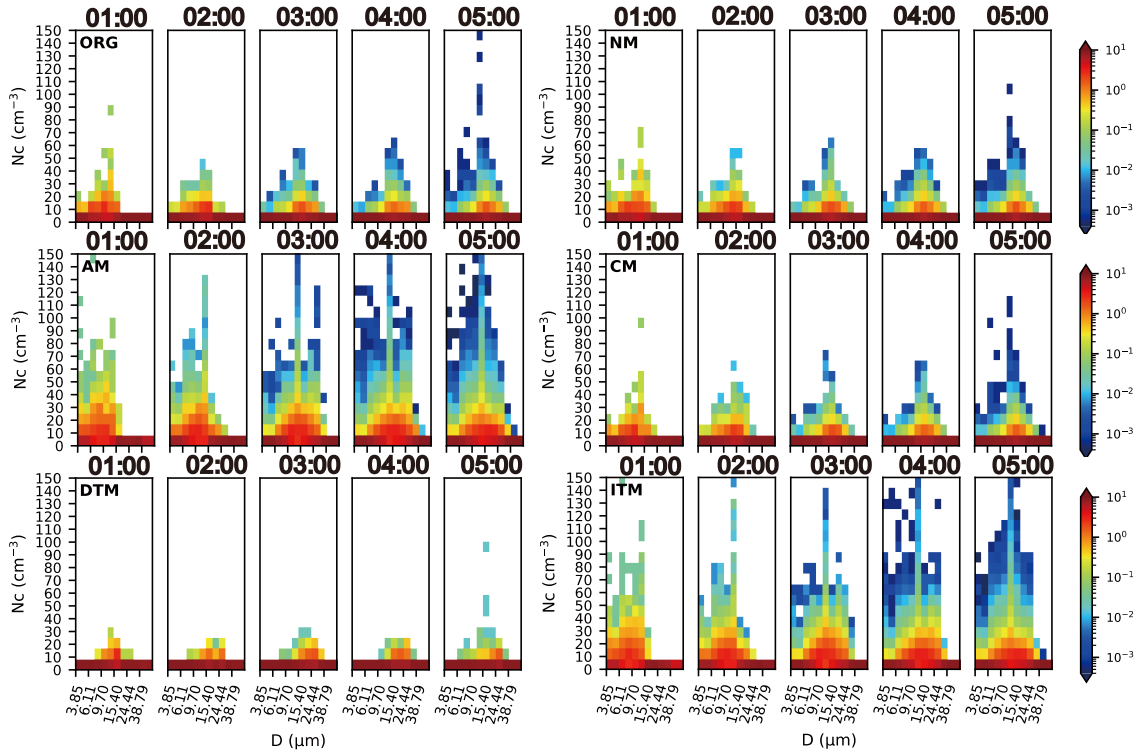
Figure 10: The variations of averaged cloud droplet number concentration (N_c , in cm^{-3}) with time (UTC) and altitude (km) within the study area of different experiments.

275

3.2.2 Cloud Droplet Size Distribution

Figure 11 represents the hourly probability distribution of N_c concerning D . As the cloud system develops, the cloud droplet spectrum widens and exhibits a unimodal distribution. When aerosol concentration increases, the cloud droplet spectrum broadens earlier, and the maximum N_c appears in the AM and ITM experiments. Additionally, the distribution characteristic of the droplet spectrum differs among the experiments. The AM and ITM experiments have their peaks in the 9-15 μm size range, while the NM and CM experiments have their peaks concentrated in the 15-24 μm size range. Meanwhile, with aerosol concentration decreased in the DTM experiment, a tendency of spectrum broadening is observed. However, the spectrum width is smaller than that in the control experiment, and the N_c is lower.

This analysis shows that increased aerosol concentration promotes cloud development and leads to an earlier widening of
 285 the cloud droplet spectrum. The increase in accumulation mode aerosols tends to increase the number concentration of small-
 sized cloud droplets. In contrast, an increase in nucleation and coarse mode aerosols favors the production of large-size cloud
 droplets. In the NM experiment, although the particle size of nucleation mode aerosols is small, the increase in aerosol
 concentration still leads to an increase in cloud droplet number concentration because aerosol particle sizes follow a normal
 distribution in the WRF-SBM scheme. Therefore, aerosol particles with larger sizes within the nucleation mode range can still
 290 participate in cloud droplet activation.



295 **3.3 Analysis of Cloud Droplet Spectrum Characteristics**

3.3.1 Vertical profiles of cloud droplet spectrum characteristics

To analyse the impact of aerosols on cloud droplet spectrum and cloud microphysical processes, Figure 12-14 given out the variations of hourly averaged ε , cloud-rain auto-conversion intensity (T), and Rv with altitude. The T value represents the probability of auto-conversion occurrence, which can be used to assess the intensity of collision-coalescence processes during cloud and precipitation (Liu et al., 2005, 2006). In the early development stage, the collision-coalescence intensity within the cloud is low. As the cloud system develops, at the vigorous development stage, the T value increases significantly, and the intensity increases with altitude. The intense collision-coalescence processes (with T values > 0.5) are primarily located in the middle to upper parts of the cloud, consistent with the distribution trend of Rv with altitude. It can be found from Figure 13 that the relative dispersion ε does not change monotonically with Rv or T. The correlation between them will be discussed in the next section.

Compared to the control experiment, the ITM and AM experiments have significantly smaller Rv values, resulting in smaller cloud droplet sizes and lower collision-coalescence intensities than the other experiments. When the aerosol concentration decreases, the Rv in the DTM experiment increases, leading to higher collision - coalescence intensity with respect to other experiments. Additionally, fewer small cloud droplets are activated due to the lower aerosol concentration in the DTM experiment, resulting in lower relative dispersion of cloud droplet spectrum than the other experiments.

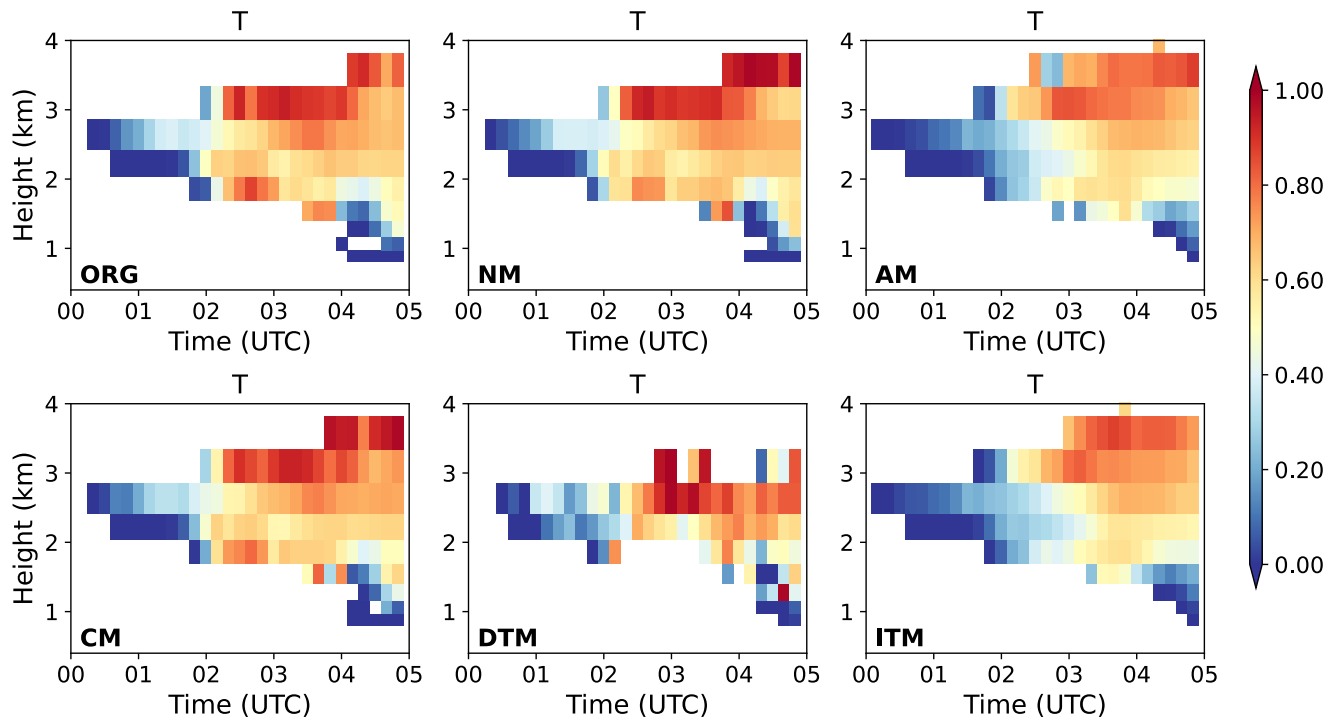
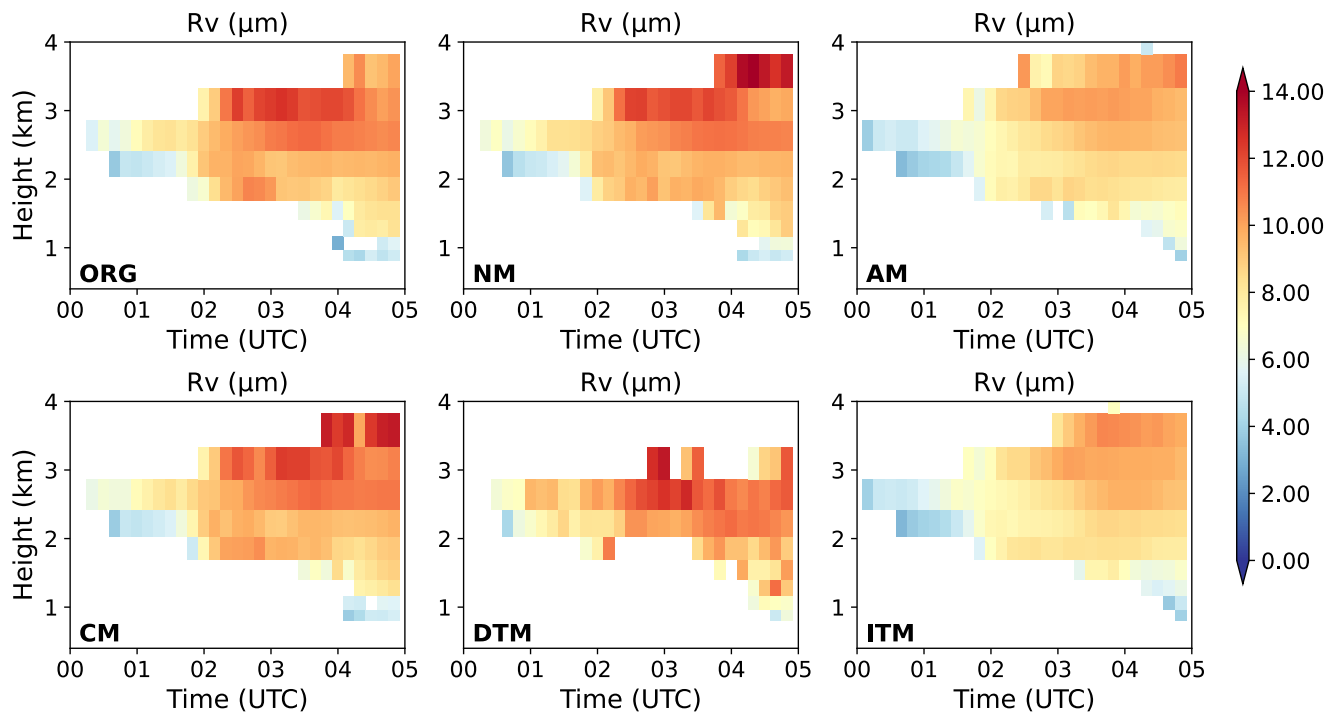


Figure 12: Distribution of cloud droplet collision-coalescence intensity (T) over time (UTC) and altitude (km). The color shading indicates the collision-coalescence intensity values.



315 **Figure 13: Distribution of cloud droplet volume-weighted mean diameter (R_v , in μm) over time (UTC) and altitude (km). The color shading indicates the magnitude of R_v values.**

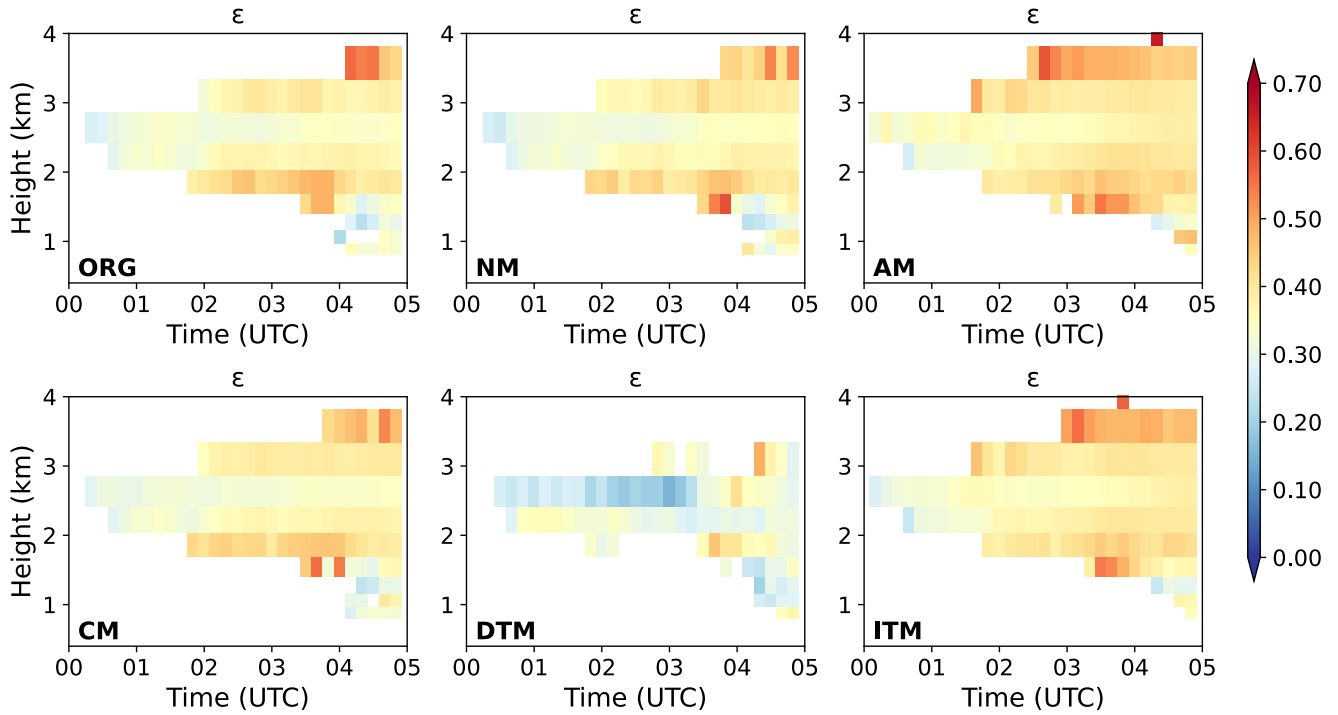


Figure 14: Distribution of relative dispersion (ϵ) of cloud droplet spectrum over time (UTC) and altitude (km). The color shading indicates the magnitude of relative dispersion values.

320 3.3.2 Relationship between ϵ -Rv

Figure 15 reflects the correlation between ϵ and Rv in experiments involving changes in concentration of aerosol modes within the cloud area from 01:00 to 05:00, illustrating the variation of ϵ during the growth of cloud droplet sizes. Fbs indicates the activation intensity corresponding to the fitted correlation in specific droplet size ranges. The ϵ -Rv correlation coefficient table is in the Supplement (Table S1). It is shown that ϵ does not vary monotonically with Rv. There is a significant transition in

325 cloud droplet collision-coalescence intensity around 8 μm radius of cloud droplet. When the Rv is smaller than 8 μm , cloud droplet growth mainly depends on the condensation process. At this stage, there exists a critical radius (R_c) of 4.2 μm . When $R_v < 4.2 \mu\text{m}$, ϵ shows a positive correlation with Rv. While $R_v > 4.2 \mu\text{m}$, ϵ shows a negative correlation with Rv. This trend is close to Lu et al. (2020), but with the value of R_c differs. Among the experiments, increased aerosol concentration enhances

the positive correlation between ε and R_v with $R_v < 4.2 \mu\text{m}$. In the ITM and AM experiments, when R_v is between $4.2\mu\text{m}$ and $8\mu\text{m}$, the negative correlation trend changes to a positive one. In contrast, decreasing aerosol concentration strengthens the negative correlation trend between ε and R_v within the same size range ($4.2 \mu\text{m} < R_v < 8 \mu\text{m}$).

Cloud droplets primarily grow through condensation within the radius range (R_v) of $2\text{--}8 \mu\text{m}$. Figure 16 illustrates the variation of cloud droplet number concentration (N_c) with R_v during the same stage as the ε - R_v correlation, reflecting the concurrent changes in N_c during the growth of cloud droplet sizes. As shown in Figure 16, when R_v is less than $4.2 \mu\text{m}$, accompanied by higher intensity of cloud droplet activation, N_c increases with R_v , and ε shows a positive correlation with R_v . When R_v ranges between 4.2 and $8 \mu\text{m}$, strong collision-coalescence processes have not yet been initiated, and activation intensity is lower. At this stage, N_c does not exhibit significant changes with increasing R_v . Due to the negative correlation between condensation growth efficiency and droplet size, smaller droplets grow rapidly through condensation, whereas larger droplets experience slower growth rate. As R_v increases, ε exhibits a negative correlation with R_v , leading to a more uniform droplet size distribution and a narrower cloud droplet spectrum. This finding aligns with the results of Liu et al. (2006) and Peng et al. (2007). When R_v exceeds $8 \mu\text{m}$, as R_v increases, higher collision-coalescence intensity rapidly depletes smaller droplets (Figure 16), with ε shows a converging trend, ultimately approaching the range of $0.3\text{--}0.4$, consistent with the findings of Lu et al. (2020).

For the sensitivity experiments, an increase in aerosol concentration enhances the activation of cloud droplets, enhancing the positive correlation between ε and R_v when $4.2 < R_v < 8 \mu\text{m}$. Among different aerosol modes, an increase in accumulation mode aerosol contributes to the prolonged maintenance of cloud droplet activation and significantly increases N_c (Figure 16). When $4.2 < R_v < 8 \mu\text{m}$, ε shows a positive correlation with R_v . However, when cloud droplet size increases above $8 \mu\text{m}$, cloud droplet collision-coalescence intensity increases with particle size, while cloud droplet number concentration decreases as R_v increases. Therefore, in this situation, dominant cloud droplet coalescence promotes the rapid growth of cloud droplet size,

350 increasing large-sized cloud droplets while simultaneously consuming small-sized cloud droplets. As a result, ε tends to converge with droplet size.

As it is shown in Figure 16 that the correlation between N_c and cloud microphysical processes is more complex. Regions with the same N_c may be dominated by condensation growth or coalescence processes. Furthermore, the ε - N_c correlation, which is significantly influenced by cloud droplet activation, condensation, and collision-coalescence processes, may exhibit
 355 even more complex variations.

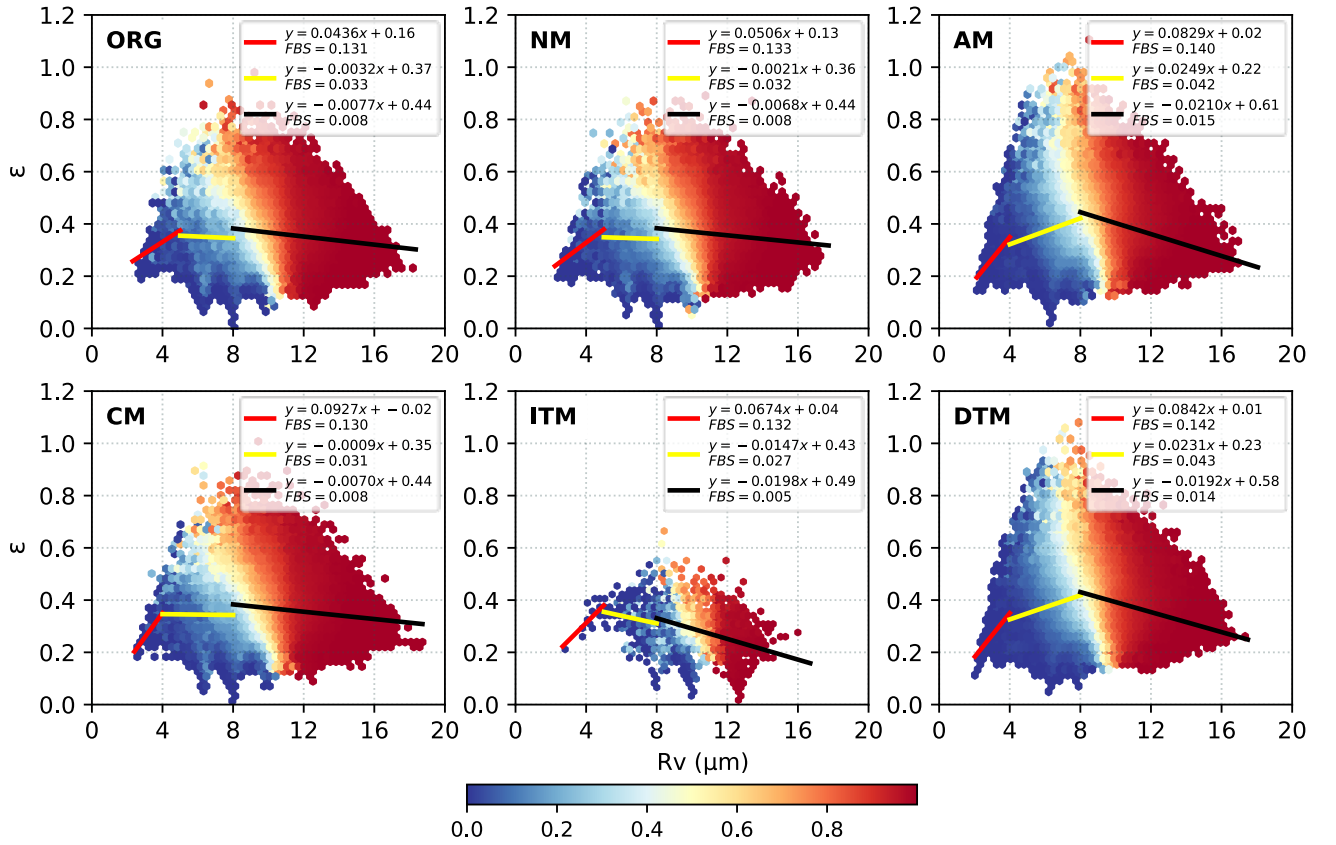


Figure 15: The variation of relative dispersion (ε) of cloud droplet spectrum against the cloud droplet volume-weighted radius (R_v , in μm) for different experiments. FBS indicates the cloud droplet activation intensity, and the shading represents the coalescence intensity.

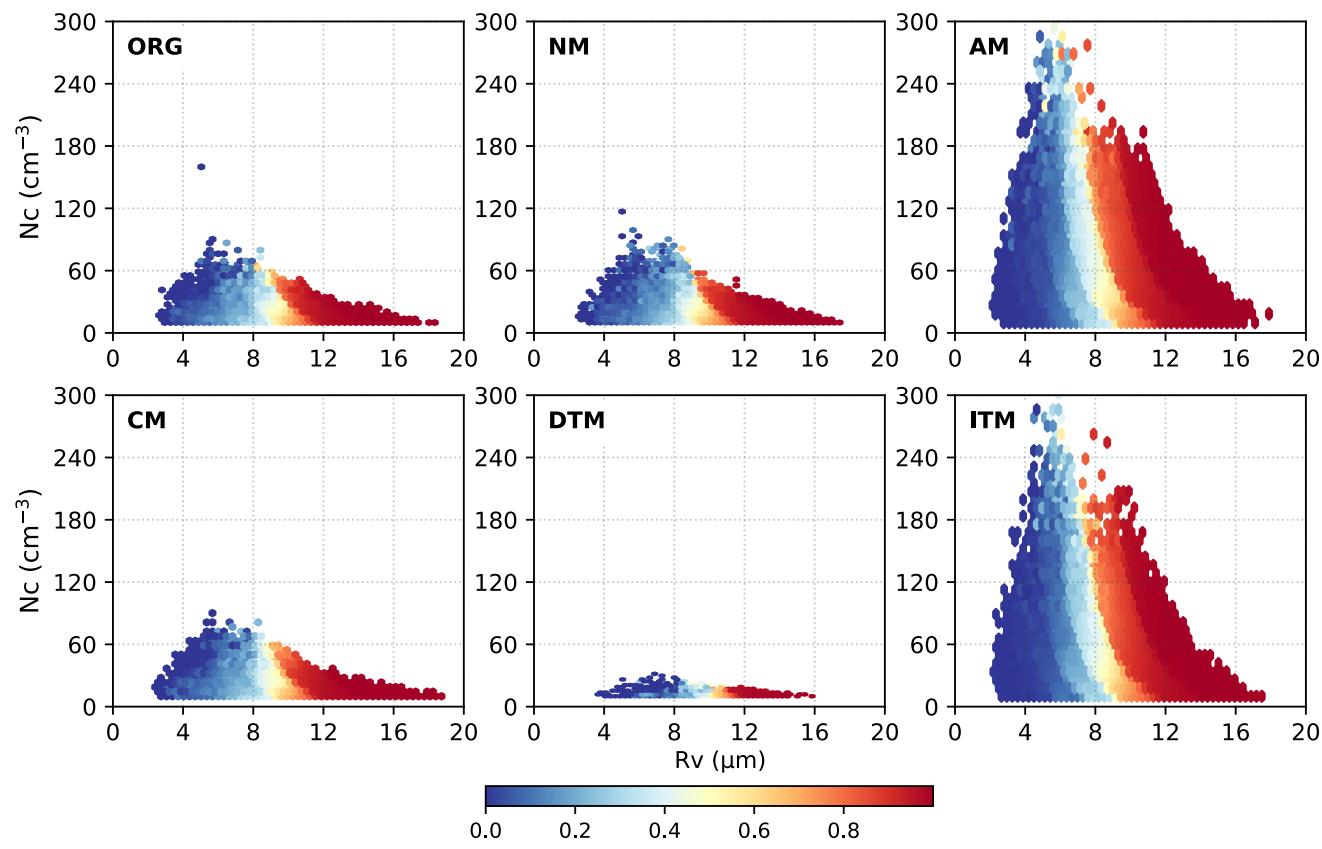
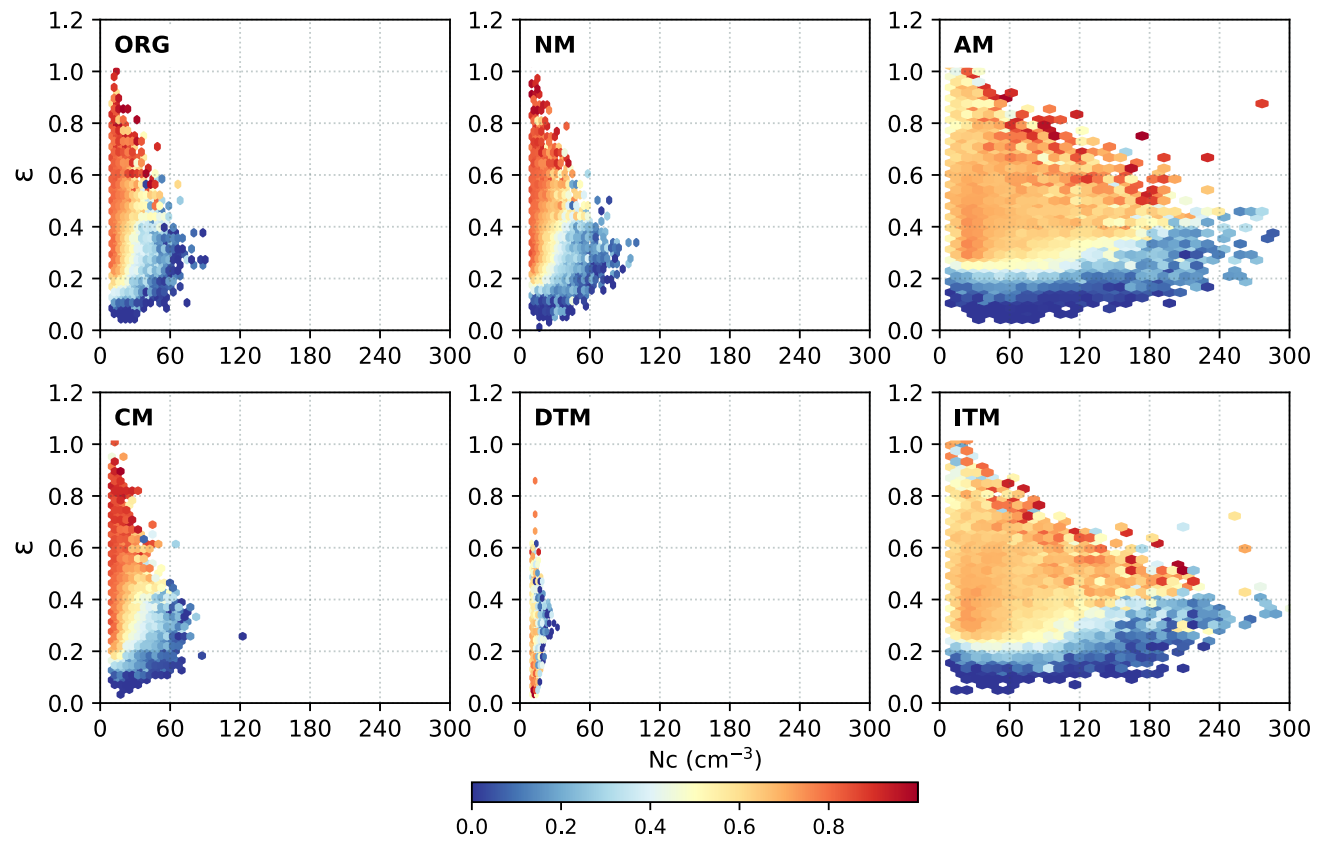


Figure 16: The variation of cloud droplet number concentration (N_c , in cm^{-3}) against the cloud droplet volume-weighted radius (R_v , in μm) for different experiments. The shading represents the coalescence intensity.

3.3.3 Relationship between ε - N_c

Figure 17 shows the relationship between ε and N_c in experiments involving changes in aerosol concentration modes within the cloud area from 01:00 to 05:00. As shown in Figure 17 as N_c increases, ε tends to converge, consistent with the findings of Zhao et al. (2006) and Jin et al. (2021). Additionally, the coalescence intensity does not significantly impact the ε - N_c correlation. With increased coalescence intensity, the dispersion of ε in the low N_c region decreases, but the ε - N_c relationship still shows a converging trend.

370 Compared to the control experiment, changes in aerosol concentration did not affect the ε -Nc correlation. When the aerosol concentration increased, Nc significantly increased, and in the AM and ITM experiments, the dispersion of ε slightly increased in the low coalescence intensity region. On the other hand, a decrease in aerosol concentration led to a significant reduction in Nc and increased cloud droplet size. In the region with $T > 0.8$, the dispersion of ε was higher.



375 **Figure 17: The variation of cloud droplet spectral relative dispersion (ε) against cloud droplet number concentration (N_c , in cm^{-3}). The shading represents the coalescence intensity.**

4 Discussion

In this study, the increase in coarse-mode aerosol concentration resulted in an increase in R_v and enhanced collision-coalescence intensity, consistent with the findings of Liu et al. (2022). However, unlike Liu et al. (2022), the increase in

380 nucleation-mode aerosol concentration in this study also promoted the early development of cloud tops above 3 km. Compared to the control experiment, both R_v and collision-coalescence intensity at the cloud top region were enhanced. This difference may stem from the classification of aerosol particle sizes; in the WRF-SBM scheme, the distribution of different aerosol modes is assumed to follow a normal distribution. Therefore, for the nucleation mode, some aerosol particles also reach the size scale of the accumulation mode, promoting an increase in N_c and a rise in T values.

385 Moreover, the relationship between ε and cloud microphysical properties differs from previous studies. In this study, ε shows a convergence trend as N_c increases, and changes in aerosol concentration do not alter this trend but rather affect the degree of dispersion, like the findings of Deng et al. (2009) and Yu et al. (2018). In contrast, study on non-precipitating stratiform clouds in northern China using aircraft observational data (Ma et al., 2010) shown that with an increase in aerosol concentration, ε tended to decrease with increasing N_c , whereas Anil et al. (2016) observed the opposite trend, with ε showing
390 a positive correlation with N_c .

The complex variations in the ε - N_c relationship are mainly due to the sensitivity of N_c and ε to many microphysical processes, such as updraft strength, aerosol properties, or condensation-coalescence processes (Lu et al., 2012; Peng et al., 2007). During the fitting process of the ε - N_c relationship, it is challenging to determine the corresponding relationship between N_c and cloud microphysical processes. In regions with low N_c , it may correspond to strong collision/coalescence initiation
395 zones, while in regions with high N_c , it may be in the condensation/coalescence dominant zone. As Liu et al. (2008) and Tas et al. (2012) have stated, compared to N_c , R_v considers the synergistic relationship between N_c and water content, providing a more explicit mapping to cloud microphysical processes. Therefore, this study explored the ε - R_v relationship to provide a more systematic understanding of the stratiform warm clouds in Eastern China. The ε - R_v correlation is summarized in Figure
18.

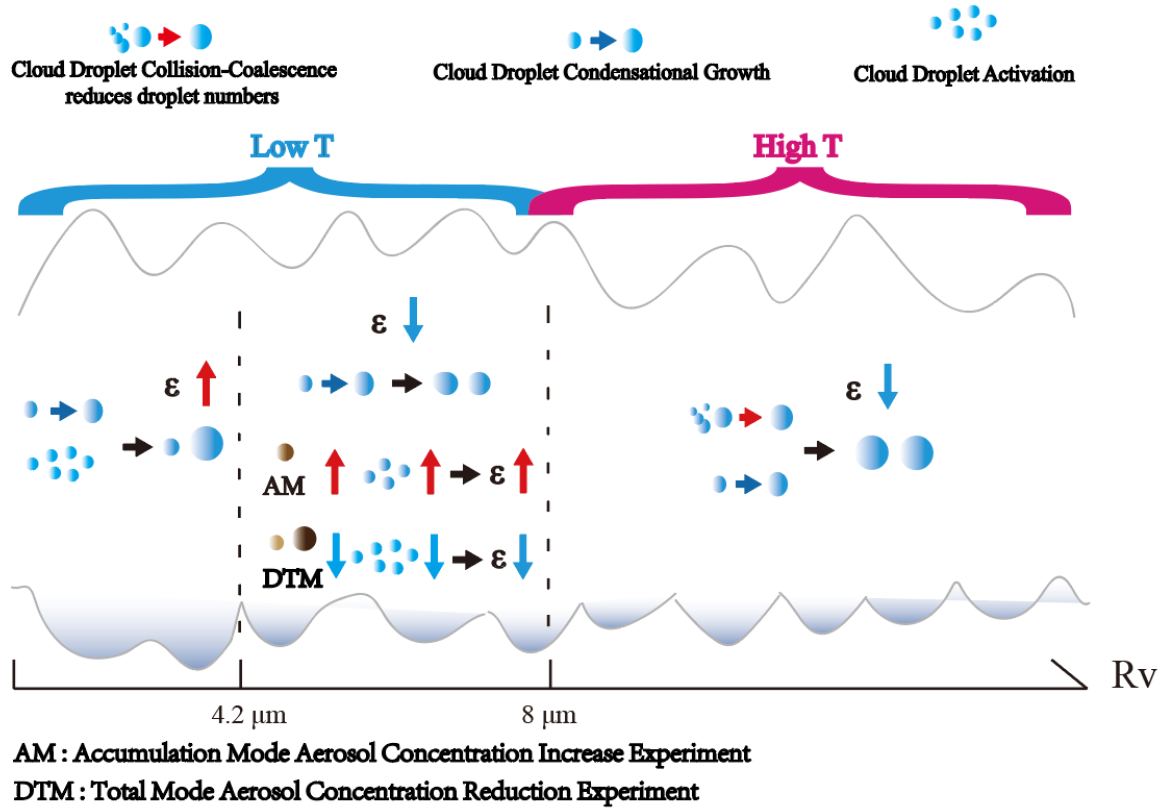


Figure 18: Correlation Mechanism between ϵ and R_v .

5 Conclusions

This study used the SBM-FAST bin scheme in the WRF model to simulate a warm cloud process in Jiangxi, China. Numerical experiments were further conducted to investigate the impact of changes in nucleation mode, accumulation mode, coarse mode, and total aerosol concentrations on the macroscopic and microscopic characteristics of warm clouds. The variations in cloud microphysical parameters with aerosol concentrations were analysed, the ϵ - R_v and ϵ - N_c relationships were fitted to explore the influence of microphysical processes on ϵ . Specific conclusions are as follows:

(1) The numerical simulation with bin microphysics scheme reproduces warm clouds' macro- and microscopic characteristics in Jiangxi, China. As the cloud system develops, R_v and T values gradually increase. Vertically, R_v increases

410 with height, and T also strengthens synchronously with the enlargement of cloud droplet size. The relationship between ε and R_v is not strictly monotonic; as R_v increases, ε initially increases and then decreases. Furthermore, it is found that variations in aerosol concentrations exert a significant influence on cloud development. With an increase in the aerosol concentration of any mode, the cloud droplet spectrum widens earlier. Specifically, higher aerosol concentrations promote cloud growth, increasing cloud-top height. In comparison, lower aerosol concentrations impede cloud droplet activation, decreasing the
415 concentration of cloud droplets and leading to a notable reduction in ε and increased R_v and higher T values.

(2) In contrast, different modes of aerosol concentration variations impact cloud microphysical properties differently. An increase in accumulation mode aerosol tends to increase the concentration of small-size cloud droplets, leading to decreased R_v and a lower collision and coalescence intensity concerning the control experiment. An increase in nucleation mode and coarse mode aerosols favors the production of large cloud droplets. As a result, the increase in accumulation mode aerosol has
420 the most significant impact on N_c enhancement. On the other hand, increases in nucleation mode and coarse mode aerosol concentrations result in an increase in R_v and an enhancement of collision and coalescence intensity.

(3) The variation of ε in the cloud is closely related to cloud microphysical processes. Fitting the ε with R_v and N_c reveals that as R_v increases, the correlation between ε and R_v changes from positive to negative, eventually converging. This transformation is mainly related to cloud droplet activation, condensation, and collision-coalescence processes within the cloud.
425 When T values are less than 0.5, as cloud droplet condensation growth becomes more active and nucleation weakens, the cloud droplet spectrum relative dispersion transitions from an increasing trend to a decreasing trend with the increase in R_v . With the enhanced coalescence between cloud droplets, ε primarily decreases with the increase in R_v . Increasing accumulation mode aerosol concentration contributes to the prolonged cloud droplet activation, enhancing the positive correlation trend between ε and R_v . On the other hand, a decrease in aerosol concentration leads to a reduction in cloud droplet activation intensity,
430 making the negative correlation trend between ε and R_v more pronounced. In addition, regardless of different T values, ε

converges with the increase in N_c . As N_c increases, ε converges to a range of 0.2-0.4. Changes in aerosol concentration for different modes do not alter the converging trend of ε with N_c but only affect the dispersion degree of ε at low N_c values.

435 Lastly, in this study, due to computational power limitations, the vertical resolution of our simulation setup is relatively coarse. Future research could consider enhancing the resolution to reveal the variations of cloud-aerosol effects more effectively within the vertical profile of clouds. Moreover, while this study has explored the effects of variations in aerosol concentrations across different modes on the macroscopic and microscopic characteristics of warm clouds, mainly focusing on the influence of these variations on the relationship between ε and cloud microphysical properties, the interaction between clouds and aerosols is a complex process influenced by multiple factors, including cloud dynamics and supersaturation levels. Therefore, future research should investigate other vital factors affecting cloud-aerosol interactions further. Additionally, 440 incorporating case studies from diverse regions could effectively reduce the regional dependency of cloud-aerosol effect research, thereby enhancing our comprehensive understanding of these complex interactions on a global scale.

6 Conflict of Interest

The authors declare that the research was conducted in the absence of any commercial or financial relationships that could be construed as a potential conflict of interest.

445 7 Acknowledgments

In addition, we acknowledge the High Performance Computing Center of Nanjing University of Information Science and Technology for their support of this work.

8 Funding

This work was supported by the National Natural Science Foundation of China (Grant Nos. 42061134009 and 41975176) and
450 2023 Jiangsu Provincial College Students' Innovative Entrepreneurial Training Program (Grant Nos.202310300108Y).

9 Data Availability Statement

The data used in this study can be accessed at the following link: <https://doi.org/10.57760/sciencedb.11210>. The data link includes the satellite-observed cloud top temperature data, WRF model simulation results, and simulated initial aerosol spectrum information used in this study.

455 The cloud top temperature data used in this study is obtained from the China National Meteorological Science Data Center. It represents the hourly cloud top temperature product observed by the VISSR instrument on the FY2G satellite. The data format is .hdf, and the temporal resolution is 30 minutes.

The WRF model simulation configurations are described in the previous section. The data format is .netcdf, and details about the data and its dimensions can be found in the data description.

460 The initial aerosol spectrum data includes the distribution information of aerosol spectra within the first hour of the simulation for one control group and five experimental groups mentioned in the article. The temporal resolution is 10 minutes. Data details can be found in the data description.

In addition, the initial fields used in the numerical simulations are based on the Fifth generation of ECMWF atmospheric reanalysis of the global climate (ERA5) hourly data on pressure levels. These data can be accessed at the following link:
465 <https://cds.climate.copernicus.eu/cdsapp#!/dataset/reanalysis-era5-pressure-levels?tab=overview>. The study utilized all height variables for every 6 hours from December 24th, 2014, 18:00 to December 25th, 2014, 06:00.

If the manuscript is accepted, the data will be publicly available through the aforementioned link (<https://doi.org/10.57760/sciencedb.11210>). To access the data, you only need to use the database link and provide your name, affiliation, and purpose of the data request to the authors for download.

470 10 References

- Anil Kumar, V. et al.: Investigation of aerosol indirect effects on monsoon clouds using ground-based measurements over a high-altitude site in Western Ghats, *Atmospheric Chemistry and Physics*, 16(13), pp. 8423–8430. doi:10.5194/acp-16-8423-2016, 2016.
- Cecchini, M.A. et al.: Sensitivities of amazonian clouds to aerosols and updraft speed, *Atmospheric Chemistry and Physics*, 17(16), pp. 10037–10050. doi:10.5194/acp-17-10037-2017, 2017.
- 475 Chandrakar, K.K. et al.: Aerosol indirect effect from turbulence-induced broadening of cloud-droplet size distributions, *Proceedings of the National Academy of Sciences*, 113(50), pp. 14243–14248. doi:10.1073/pnas.1612686113, 2016.
- Chandrakar, K.K., Cantrell, W. and Shaw, R.A.: Influence of turbulent fluctuations on cloud droplet size dispersion and aerosol indirect effects, *Journal of the Atmospheric Sciences*, 75(9), pp. 3191–3209. doi:10.1175/jas-d-18-0006.1, 2018.
- 480 Chen, J. et al.: New understanding and quantification of the regime dependence of aerosol-cloud interaction for studying aerosol indirect effects, *Geophysical Research Letters*, 43(4), pp. 1780–1787. doi:10.1002/2016gl067683, 2016.
- Desai, N. et al.: Search for microphysical signatures of stochastic condensation in marine boundary layer clouds using airborne digital holography, *Journal of Geophysical Research: Atmospheres*, 124(5), pp. 2739–2752. doi:10.1029/2018jd029033, 2019.
- 485 Fan J, Leung L R, Li Z, et al. Aerosol impacts on clouds and precipitation in eastern China: Results from bin and bulk microphysics [J]. *Journal of Geophysical Research: Atmospheres*, 117(D16), doi: 10.1029/2011JD016537, 2012.

- Flossmann, A.I. and Wobrock, W.: A review of our understanding of the aerosol–cloud interaction from the perspective of a bin resolved cloud scale modelling, *Atmospheric Research*, 97(4), pp. 478–497. doi:10.1016/j.atmosres.2010.05.008, 2010.
- 490 Grosvenor, D. P., Sourdeval, O., Zuidema, P., Ackerman, A., Alexandrov, M. D., Bennartz, R., et al.: Remote sensing of droplet number concentration in warm clouds: A review of the current state of knowledge and perspectives. *Reviews of Geophysics*, 56, 409– 453. <https://doi.org/10.1029/2017RG000593>, 2018.
- Han, B. et al.: Cloud-Resolving Model Intercomparison of an MC3E squall line case: Part II. Stratiform precipitation properties, *Journal of Geophysical Research: Atmospheres*, 124(2), pp. 1090–1117. Available at: <https://doi.org/10.1029/2018jd029596>, 2019.
- 495 <https://doi.org/10.1029/2018jd029596>, 2019.
- Hersbach, H., Bell, B., Berrisford, P., Biavati, G., Horányi, A., Muñoz Sabater, J., Nicolas, J., Peubey, C., Radu, R., Rozum, I., Schepers, D., Simmons, A., Soci, C., Dee, D., Thépaut, J-N.: ERA5 hourly data on pressure levels from 1940 to present. Copernicus Climate Change Service (C3S) Climate Data Store (CDS), DOI: 10.24381/cds.bd0915c6, 2023.
- Iltoviz, E. et al.: Effect of aerosols on freezing drops, hail, and precipitation in a midlatitude storm, *Journal of the Atmospheric Sciences*, 73(1), pp. 109–144. doi:10.1175/jas-d-14-0155.1, 2015.
- 500 *Sciences*, 73(1), pp. 109–144. doi:10.1175/jas-d-14-0155.1, 2015.
- Jensen, J.B. and Nugent, A.D.: Condensational growth of drops formed on giant sea-salt aerosol particles, *Journal of the Atmospheric Sciences*, 74(3), pp. 679–697. doi:10.1175/jas-d-15-0370.1, 2017.
- Jin Yuchen, Niu Shengjie, Lü Jingjing, et al.: Study of the Microphysical Structural Characteristics and Cloud–Rain Autoconversion Threshold Function of Stratiform Warm Clouds in Jiangxi [J]. *Chinese Journal of Atmospheric Sciences*, 45(5): 981–993. doi: 10.3878/j.issn.1006-9895.2102.20166, 2021.
- 505 45(5): 981–993. doi: 10.3878/j.issn.1006-9895.2102.20166, 2021.
- Kant, S., Panda, J. and Gautam, R.: A seasonal analysis of aerosol-cloud-radiation interaction over Indian region during 2000–2017, *Atmospheric Environment*, 201, pp. 212–222. doi:10.1016/j.atmosenv.2018.12.044, 2019.

- Khain, A. and Sednev, I.: Simulation of precipitation formation in the Eastern Mediterranean Coastal Zone using a spectral microphysics cloud ensemble model, *Atmospheric Research*, 43(1), pp. 77–110. Available at: [https://doi.org/10.1016/s0169-8095\(96\)00005-1](https://doi.org/10.1016/s0169-8095(96)00005-1), 1996.
- Khain, A. et al.: Notes on the state-of-the-art numerical modeling of Cloud Microphysics, *Atmospheric Research*, 55(3-4), pp. 159–224. Available at: [https://doi.org/10.1016/s0169-8095\(00\)00064-8](https://doi.org/10.1016/s0169-8095(00)00064-8), 2000.
- Khain A P, Rosenfeld D, Pokrovsky A, et al.: Effects of Atmospheric Aerosols on Precipitation From Deep Convective Clouds As Seen From Simulations Using A Spectral Microphysics Cloud Model[J]. Available at: 2002EGSGA.27.6326K, 2002.
- Khain, A., Rosenfeld, D. and Pokrovsky, A.: Aerosol impact on the dynamics and microphysics of deep convective clouds. *Quarterly Journal of the Royal Meteorological Society: A journal of the atmospheric sciences, applied meteorology and physical oceanography*, 131(611), pp.2639-2663, 2005.
- Khain, A. and Lynn, B.: Simulation of a supercell storm in clean and dirty atmosphere using weather research and forecast model with spectral bin Microphysics, *Journal of Geophysical Research*, 114(D19). Available at: <https://doi.org/10.1029/2009jd011827>, 2009.
- Kovačević, N.: Hail suppression effectiveness for varying solubility of natural aerosols in water, *Meteorology and Atmospheric Physics*, 131(3), pp. 585–599. doi:10.1007/s00703-018-0587-4, 2018.
- Kumar, B. et al.: Cloud-edge mixing: Direct numerical simulation and observations in Indian Monsoon clouds, *Journal of Advances in Modeling Earth Systems*, 9(1), pp. 332–353. doi:10.1002/2016ms000731, 2017.
- Lau, K.M. and Wu, H.T.: Warm rain processes over tropical oceans and climate implications, *Geophysical Research Letters*, 30(24). Available at: <https://doi.org/10.1029/2003gl018567>, 2003.
- Lerach, D.G. and Cotton, W.R.: Simulating southwestern U.S. desert dust influences on supercell thunderstorms, *Atmospheric Research*, 204, pp. 78–93. doi:10.1016/j.atmosres.2017.12.005, 2018.

- Liu, F. et al.: Opposing comparable large effects of fine aerosols and coarse sea spray on marine warm clouds, *Communications Earth & Environment*, 3(1). doi:10.1038/s43247-022-00562-y, 2022.
- 530 Liu, G.: Retrieval of cloud droplet size from visible and microwave radiometric measurements during INDOEX: Implication to aerosols' indirect radiative effect, *Journal of Geophysical Research*, 108(D1). doi:10.1029/2001jd001395, 2003.
- Liu, Y. and Daum, P.H.: Indirect warming effect from dispersion forcing, *Nature*, 419(6907), pp. 580–581. doi:10.1038/419580a, 2002.
- 535 Liu, Y.: Size truncation effect, threshold behavior, and a new type of autoconversion parameterization, *Geophysical Research Letters*, 32(11). doi:10.1029/2005gl022636, 2005.
- Liu, Y. et al.: Generalized threshold function accounting for effect of relative dispersion on threshold behavior of autoconversion process, *Geophysical Research Letters*, 33(11). doi:10.1029/2005gl025500, 2006.
- Liu, Y. et al.: Dispersion bias, dispersion effect, and the aerosol–cloud conundrum, *Environmental Research Letters*, 3(4), p. 045021. doi:10.1088/1748-9326/3/4/045021, 2008.
- 540 Liu, Y. et al.: Tibetan Plateau driven impact of Taklimakan dust on northern rainfall, *Atmospheric Environment*, 234, p. 117583. doi:10.1016/j.atmosenv.2020.117583, 2020.
- Lu, C. et al.: Observed impacts of vertical velocity on cloud microphysics and implications for aerosol indirect effects, *Geophysical Research Letters*, 39(21). doi:10.1029/2012gl053599, 2012.
- 545 Lu, C. et al.: Empirical relationship between entrainment rate and microphysics in cumulus clouds', *Geophysical Research Letters*, 40(10), pp. 2333–2338. doi:10.1002/grl.50445, 2013.
- Lu, C. et al.: Reconciling contrasting relationships between relative dispersion and volume-mean radius of cloud droplet size distributions, *Journal of Geophysical Research: Atmospheres*, 125(9). doi:10.1029/2019jd031868, 2020.

- Lu, C. S., & Xu, X. Q.: Research Progress on Cloud Entrainment-Mixing Processes. *Torrential Rain and Disasters (in China)*,
550 40(3), 271-279. DOI: 10.3969/j.issn.1004-9045.2021.03.005, 2021.
- Ma, J. et al.: Strong air pollution causes widespread haze-clouds over China, *Journal of Geophysical Research*, 115(D18).
doi:10.1029/2009jd013065, 2010.
- Morrison, H. et al.: Broadening of modeled cloud droplet spectra using bin microphysics in an Eulerian spatial domain, *Journal
of the Atmospheric Sciences*, 75(11), pp. 4005–4030. doi:10.1175/jas-d-18-0055.1, 2018.
- 555 Pandithurai, G. et al.: Aerosol effect on droplet spectral dispersion in warm continental cumuli, *Journal of Geophysical
Research: Atmospheres*, 117(D16). doi:10.1029/2011jd016532, 2012.
- Peng, Y. et al.: An investigation into the aerosol dispersion effect through the activation process in marine stratus clouds,
Journal of Geophysical Research, 112(D11). doi:10.1029/2006jd007401, 2007.
- Pinsky, M. and Khain, A.: Theoretical Analysis of the Entrainment–mixing process at cloud boundaries. part I: Droplet size
560 distributions and humidity within the interface zone, *Journal of the Atmospheric Sciences*, 75(6), pp. 2049–2064.
doi:10.1175/jas-d-17-0308.1, 2018.
- Prabha, T.V. et al.: Spectral width of premonsoon and monsoon clouds over Indo-Gangetic Valley, *Journal of Geophysical
Research: Atmospheres*, 117(D20). doi:10.1029/2011jd016837, 2012.
- Qian Y, Gong D, Fan J, et al. Heavy pollution suppresses light rain in China: Observations and modeling [J]. *Journal of
565 Geophysical Research: Atmospheres*, 114(D7), doi: 10.1029/2008jd011575, 2009.
- Rosenfeld, D., Rudich, Y. and Lahav, R.: Desert dust suppressing precipitation: A possible desertification feedback loop,
Proceedings of the National Academy of Sciences, 98(11), pp. 5975–5980. doi:10.1073/pnas.101122798, 2001.

- Rotstayn, L.D. and Liu, Y.: Sensitivity of the first indirect aerosol effect to an increase of cloud droplet spectral dispersion with droplet number concentration, *Journal of Climate*, 16(21), pp. 3476–3481. doi:10.1175/1520-0442(2003)016<3476: sotfia>2.0.co;2, 2003.
- 570 Rotstayn, L.D. and Liu, Y.: Cloud droplet spectral dispersion and the indirect aerosol effect: Comparison of two treatments in a GCM, *Geophysical Research Letters*, 36(10). doi:10.1029/2009gl038216, 2009.
- Seifert, A., Nuijens, L. and Stevens, B.: Turbulence effects on warm-rain autoconversion in precipitating shallow convection. *Quarterly Journal of the Royal Meteorological Society*, 136(652), pp.1753-1762, 2010.
- 575 Shpund, J. et al.: Simulating a mesoscale convective system using WRF with a new spectral bin Microphysics: 1: Hail vs graupel, *Journal of Geophysical Research: Atmospheres*, 124(24), pp. 14072–14101. doi:10.1029/2019jd030576, 2019.
- Tas, E., Koren, I. and Altaratz, O.: On the sensitivity of droplet size relative dispersion to warm cumulus cloud evolution, *Geophysical Research Letters*, 39(13). doi:10.1029/2012gl052157, 2012.
- Tas, E. et al.: The relative dispersion of cloud droplets: Its robustness with respect to key cloud properties, *Atmospheric Chemistry and Physics*, 15(4), pp. 2009–2017. doi:10.5194/acp-15-2009-2015, 2015.
- 580 Wang Fei, Lu Chunsong.: Advances of Theoretical, Observational, and Numerical Studies on Relative Dispersion of Cloud Droplet Spectral (in China). *Plateau Meteorology*. DOI: 10. 7522/j. issn. 1000-0534. 00067, 2022.
- Wang, F. et al.: An airborne study of the aerosol effect on the dispersion of cloud droplets in a drizzling marine stratocumulus cloud over eastern China, *Atmospheric Research*, 265, p. 105885. doi:10.1016/j.atmosres.2021.105885, 2022.
- 585 Wang, X. et al.: A study of shallow cumulus cloud droplet dispersion by large eddy simulations, *Acta Meteorologica Sinica*, 25(2), pp. 166–175. doi:10.1007/s13351-011-0024-9, 2011.
- Wang, Y. et al.: An observational study on cloud spectral width in North China, *Atmosphere*, 10(3), p. 109. doi:10.3390/atmos10030109, 2019.

- Wang, Y. et al.: Diverse dispersion effects and parameterization of relative dispersion in urban fog in eastern China, *Journal of Geophysical Research: Atmospheres*, 128(6). doi:10.1029/2022jd037514, 2023.
- Wehbe, Y., Temimi, M. and Adler, R.F.: Enhancing precipitation estimates through the fusion of weather radar, satellite retrievals, and surface parameters, *Remote Sensing*, 12(8), p. 1342. doi:10.3390/rs12081342, 2020.
- Xie, X. N., Liu, X. D., & Wang, Z. S.: Research Progress on the Impact of Cloud Droplet Spectrum Dispersion on Aerosol Indirect Effects (in China). *Journal of Earth Environment*, 6(2), 8. DOI: 10.7515/JEE201502008, 2015.
- Xie, X. et al.: Sensitivity study of cloud parameterizations with relative dispersion in CAM5.1: Impacts on aerosol indirect effects, *Atmospheric Chemistry and Physics*, 17(9), pp. 5877–5892. doi:10.5194/acp-17-5877-2017, 2017.
- Yang, F. et al.: Evaluation of multiple forcing data sets for precipitation and shortwave radiation over major land areas of China, *Hydrology and Earth System Sciences*, 21(11), pp. 5805–5821. doi:10.5194/hess-21-5805-2017, 2017.
- Yang, S. et al.: Effects of aerosol number concentration and updraft velocity on relative dispersion during the collision–coalescence growth stage of warm clouds, *Atmosphere*, 14(5), p. 828. doi:10.3390/atmos14050828, 2023.
- Yin, Y. et al.: The effects of giant cloud condensation nuclei on the development of precipitation in convective clouds — a numerical study, *Atmospheric Research*, 53(1–3), pp. 91–116. doi:10.1016/s0169-8095(99)00046-0, 2000.
- Yu Guohang, Yang Suying, Hu Cheng-rong, et al.: Simulation on Impacts of Aerosol Number Concentration on Physical Characteristics of Warm Clouds during Different Growth Stages [J]. *Journal of Meteorology and Environment*, 38(3): 52-64, 2022.
- Yum, S.S. and Hudson, J.G.: Adiabatic predictions and observations of cloud droplet spectral broadness, *Atmospheric Research*, 73(3–4), pp. 203–223. doi:10.1016/j.atmosres.2004.10.006, 2005.
- Zhao, C. and Ishizaka, Y.: Modeling marine stratocumulus with a detailed microphysical scheme, *Advances in Atmospheric Sciences*, 21(1), pp. 61–74. Available at: <https://doi.org/10.1007/bf03342546>, 2004.

- 610 Zhao, C. et al.: Aircraft measurements of cloud droplet spectral dispersion and implications for indirect aerosol radiative forcing, *Geophysical Research Letters*, 33(16). doi:10.1029/2006gl026653, 2006.
- Zheng, X. et al.: Comparison of macro- and microphysical properties in precipitating and non-precipitating clouds over Central-eastern China during warm season, *Remote Sensing*, 14(1), p. 152. doi:10.3390/rs14010152, 2021.
- Zhu Lei, Lu Chunsong, Gao Sinan, Yum Seong Soo.: Spectral Width of Cloud Droplet Spectra and Its Impact Factors in Marine Stratocumulus[J]. *Chinese Journal of Atmospheric Sciences*, 44(3): 575-590. doi: 10.3878/j.issn.1006-9895.1905.19115, 2020.
- 615